This is to certify that the

thesis entitled

Quantification of In-Cylinder
Flow Characteristics With Laser
Doppler Velocimetry

presented by

John David Mueller

has been accepted towards fulfillment
of the requirements for

Master of Science degree in Mechanical Engineering

Major professor

Date May 22, 1995

# QUANTIFICATION OF IN-CYLINDER FLOW CHARACTERISTICS WITH LASER DOPPLER VELOCIMETRY

By

John David Mueller

A THESIS

Submitted to
Michigan State University
in partial fulfillment of the requirements
for the degree of

MASTER OF SCIENCE

Department of Mechanical Engineering

1995

ABSTRACT

QUANTIFICATION OF IN-CYLINDER FLOW CHARACTERISTICS WITH LASER DOPPLER VELOCIMETRY

By

John David Mueller

Velocities inside a cylinder of a Chrysler 3.5 liter, 24 valve, V-6 engine were measured using Laser Doppler Velocimetry, to determine how engine configuration affects the flow field. A three component LDV system was used to take velocity measurements. Two distinct intake/piston arrangements were studied.

Data was processed in two different formats: visual and numerical. Explorer was used to create pictures of the flow fields that were run together as a movie. FORTRAN programs were created to calculate values of velocity, vorticity, circulation, turbulent kinetic energy and tumble in each plane at each crank angle.

It was determined that the in-cylinder flow pattern is dominated by the intake effects and that the piston top designs had a minimal effect on flow. Tumble calculations were found to quantify bulk flow, circulation small flow areas, and TKE individual point characteristics. Calculations of tumble and circulation make the most distinction between flow patterns.

# ACKNOWLEDGMENTS

Many people helped to make this project a success. Thanks first to Dr. Schock and Tom Stuecken for getting the projects, keeping the Lab running and the funding coming in. Thanks to Dr. Lee for the hours of instruction and advice. Thanks to Kwang Hwang for having someone to do all those measurements with. Thanks to Mark Novak for getting things going on the Sun, being the guinea-pig on the SGI, and for all the great conversations. Thanks to the Chrysler Corporation for their financial support of this and other projects at the ERL, with special thanks to Phil Keller and Mary Chappell for their input and help. Finally, thanks to Lynnette for having the love and the patience to put up with me during the last two years here at the ERL.

# TABLE OF CONTENTS

# LIST OF TABLES

# LIST OF FIGURES

# NOMENCLATURE

Greek

| | |
|---|---|
| $\Gamma$ | circulation |
| $\gamma$ | intermediate value in circulation calculations |
| $<\rho>$ | average density |
| $\Omega_{cs}$ | crank shaft speed (radians/sec) |
| $\varpi$ | vorticity |

Arabic

| | |
|---|---|
| A | area |
| $\mathbf{b}$ | generic unit direction |
| H | angular momentum |
| M | moment of inertia |
| $\hat{n}$ | unit normal direction |
| $\mathbf{r}$ | position vector from origin |
| S | swirl number (tumble about y axis) |
| T | tumble number |
| $\hat{\mathbf{U}}$ | density weighted average velocity |
| $\bar{\mathbf{V}}$ | velocity vector |

Subscripts

| | |
|---|---|
| a | average |
| b | generic unit direction |
| r | root mean square |
| t | total |
| x, y, z | about the x, y, or z axis |

# INTRODUCTION

This study is a continuation of an investigation into how piston design and cylinder head design affect in-cylinder flow of a Chrysler 3.5 L, four-valve, V-6 spark ignition engine. Previous work at the Michigan State University Engine Research Laboratory (MSU ERL) used two and three dimensional laser Doppler velocimetry (LDV) and high speed flow visualization to examine in-cylinder flow during the intake and compression strokes, in one plane. This study continues the work by studying more configurations, and expands on the previous work by utilizing three-component LDV in two planes, and by introducing a calculation of tumble and swirl.

The automotive industry is constantly trying to improve engine performance. Increased power, better driveability, higher fuel economy, and lower emissions are needed to attract customers and meet federal regulations. The testing of new designs usually encompasses static flow testing of individual components, computer simulations, and extensive dynamometer testing. No single method of testing is complete enough and inexpensive enough to be used alone. The goal for LDV measurements is to try to quantify in-cylinder flow patterns, which would allow for prediction of engine performance without lengthy dynamometer testing.

The current standard for defining flow characteristics in an engine is through tumble and swirl. A specific engine configuration will be given a tumble and swirl number based on flow bench testing (e.g., tumble # = 2.1). Neither has a standard definition nor a standard metric. Swirl is generally described as net angular momentum about the cylinder axis, while tumble is defined as net angular momentum about the axes normal to the cylinder axis. These forms of in cylinder motion are believed to increase turbulent kinetic energy and increase the burn rate. A complete understanding how tumble & swirl affect the combustion process does not exist, but through years of experience automotive companies have been able to use these ideas to improve engine design. A better understanding of in cylinder flow structure is sought through LDV measurements.

# EXPERIMENTAL FACILITIES

## TEST RIG

A test stand consisting of a research engine, a driving motor , a quartz cylinder, a cylinder head, a lubricating system, and a speed controller was used for the experiments (Figure 1). An AVL type 520 single cylinder research engine was used to motor the pistons. The stroke and the squish height were adjusted to match the setup used by Chrysler in the actual engine. A production 3.5L V-6 engine head was used, with minor modifications. The center cylinder of the right side bank (as viewed from the front of the engine) was used for the studies. A section of the production intake manifold leading to the center cylinder was attached to the head. A straight pipe was used as an idealized exhaust runner. A 10 hp electric motor drove the AVL engine from the engine crankshaft, at a speed of 600 rpm. The entire assembly was mounted on a heavy steel bed-plate to reduce vibration. The bed-plate was placed on rubber isolation mounts to further reduce vibration transmission through the floor to the laser system.

The 96 mm bore cylinder was made of 9.5 mm thick quartz. The cylinder was polished to prevent alteration of the fringe patterns by minor surface defects. Gaskets made of Rulon-LD were placed at the contact between the cylinder and the engine head and the contact between the cylinder and the adapter plate on the AVL engine, to prevent oil leakage and chipping of the cylinder. The use of the quartz cylinder requires that non-scratching piston rings be used. Rulon-LD was used for piston rings because it will not scratch the cylinder, can withstand high temperatures and compressive loads, and

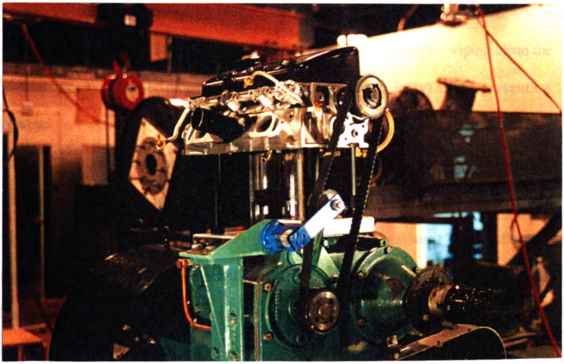

Figure 1: Test Stand.

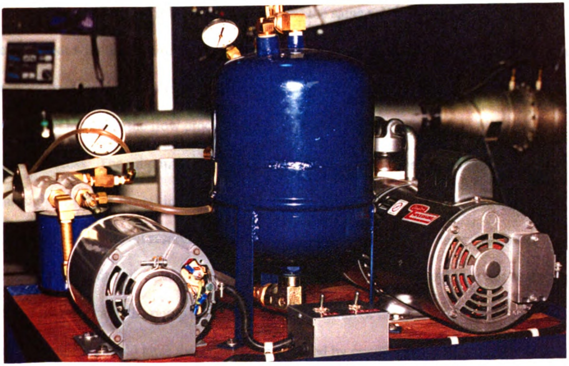

Figure 2: External Lubrication System.

requires no lubrication. The rings prevent the metal piston from making contact with and scratching the cylinder. The rings still act like standard piston rings by wiping clean the cylinder of any condensed moisture (maintaining high optical clarity) and by preventing blowby.

The engine head was modified slightly for these experiments. Since only the center cylinder was used, the front and rear cylinders' rocker arms were removed. Hoses were clamped over the oil holes in the rocker shaft to maintain oil pressure. The head's oil supply passages were threaded so that an external lubrication system could be attached. The camshaft was driven by a gear belt powered from the camshaft of the AVL engine. The four-piece AVL camshaft was modified so that the 3.5L engine cam timing could be adjusted on the auxiliary portion of the camshaft independent of the AVL cam.

The engine head lubricating oil followed the same pathways as the standard 3.5L engine, but with the oil circulated by an oil pump and vacuum system (Figure 2). This was needed because the cylinder axis was set vertically (in a car it would be at a 60 degree angle), which alters the flow process, and to keep oil return pathways from blocking optical access. The oil pump draws 10W-30 oil from the oil reservoir and pumps it through a filter, to the oil inlet port on the head. The vacuum pump creates low pressure (127 mm Hg) in the oil reservoir which draws oil and air from under the valve cover, through the oil drains on the head, into the reservoir. The vacuum sucks air out of the top of the reservoir and the pump draws oil from the bottom of the reservoir. Both the pump and the vacuum could have their flow rates adjusted by opening or closing control valves. The use of a vacuum has the advantage of reducing the chance of oil dripping into the cylinder from the valves. The suction created pulls oil out of the head, removing standing oil which could drip down the valve stems. If dripping did occur, oil would smear on the quartz and greatly reduce laser transmission through the cylinder.

## ENGINE CONFIGURATIONS

Two piston/intake configurations were examined in this study. The first, configuration M, consisted of a 50% blocked intake port and a pop-up piston (Figure 3a). The pop-up piston had a raised, rectangular center section that ran parallel to the cylinder bank, with poppet-valve notches cut into the face. Configuration M had a compression ratio of 9.5:1 and operated at a peak pressure of 195 psi when run at 600 rpm. Configuration N consisted of a standard unblocked intake port and a dish piston (Figure 3b). The piston face had a circular depression (dish) in the center and notches for valve clearance. Configuration N had a compression ratio of 9.0:1 and operated at a peak pressure of 187 psi when run at 600 rpm.

Table 1: Engine Configurations

| Configuration | Piston Head | Intake Port | Peak Pressure (psi) | Compression Ratio | RPM |
|---|---|---|---|---|---|
| M | Pop up | 50 % Blocked | 195 | 9.5 | 600 |
| N | Dish | 0 % Blocked | 187 | 9.0 | 600 |

(a)

(b)

Figure 3: Piston and intake port for (a) Configuration M and (b) Configuration N.

## THREE-COMPONENT LDV SYSTEM

The three-component laser Doppler velocimetry system consisted of an argon-ion laser, beam collimator, polarization rotators, beam splitters, beam steering and expanding lenses, focusing and receiving lenses, Bragg cells and frequency shifters, a Colorburst fiber-optic transmission unit, fiber optic probe, photodetectors, a digital burst correlator, rotating machinery resolver (RMR), traverse mechanism, and a personal computer for data acquisition (Figure 4). A multi-wavelength beam emitted from the Ar-Ion laser is used as the light source. The beam is directed into the collimator, and then separated into several

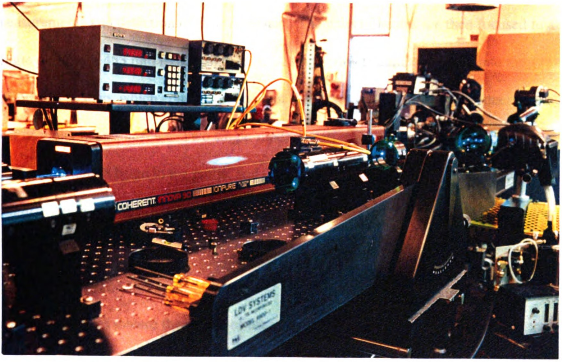


Figure 4: LDV Table.

single wavelength beams by a prism. Three beams are then selected for use, 514.5 nm (green), 488 nm (blue), 476.5 nm (violet). The green and blue beams run parallel to each other and are sent through the standard optics, while the violet beam is sent through the Colorburst system. The fiber optic system allows the violet beam to be sent through the focusing point perpendicular to the green and blue beams for the third velocity component.

Figure 5 shows a schematic of the LDV system. The green and blue beams are each split into two equal intensity beams spaced 50 mm apart. The two pairs of beams are next sent through a Bragg Cell to generate a fringe pattern in one of the beams. The frequency shifter controls the fringe pattern movement, allowing directional velocity measurements and detection of flow reversals. The pairs of beams are then focused to a single point by a 453 mm focal length lens. A single violet beam is directed into the Colorburst system, which contains in one unit the necessary components to generate the pair of violet beams needed. Two single-mode, polarization-preserving fibers each carry a single-wavelength beam to the probe, and through the focusing lens (350 mm focal length). All three pairs of beams are focused onto a single measurement volume.

The green beams measure the y-component of velocity, which is parallel to the axis of the cylinder. The blue beams measure the x-component of velocity, which is a radial direction that runs toward the source of the violet beam. The violet beams measure the z-component of velocity, which is the radial direction that runs toward the source of the blue and green beams (Figure 6). The location of the measuring volume is controlled by a traverse table control unit, which moves the table and its extension arms upon which all

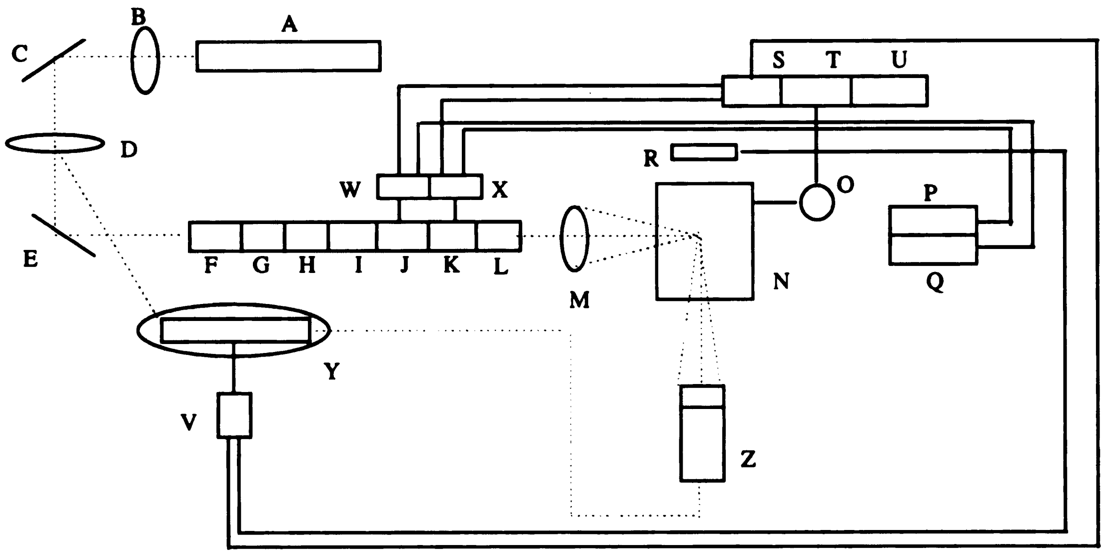


A) Argon -Ion Laser

B) Beam Collimator

C) Steering Mirror

D) Prism

E) Steering Mirror

F) Beam Splitter - 488.0 nm

G) Beam Splitter - 514.5 nm

H) Polarizer - 488.0 nm

I) Polarizer - 514.5 nm

J) Bragg Cell - 488.0 nm

K) Bragg Cell - 514.5 nm

L) Beam Stop

M) Focusing Lens

N) Catalytic Converter

O) Shaft Encoder

P) Receiving Optics - 514.5 nm

Q) Receiving Optics - 488.0 nm

R) Receiving Optics - 476.5 nm

S) IFA 750 Signal Processor

T) Rotating Machinery Resolver

U) Master Interface Unit

V) Frequency Shifter - 476.5 nm

W) Frequency Shifter - 488.0 nm

X) Frequency Shifter - 514.5 nm

Y) Colorburst

Z) Fiberoptic Probe

Figure 5. Schematic of LDV System.

the laser equipment is attached. The table is isolated from engine vibrations by rubber mounting pads placed under the base. The traverse table can measure movement to the nearest thousandth of a millimeter.

Velocity is measured by detection of the Doppler signal given off by particles passing through the three sets of fringe patterns in the measurement volume. For this study a 1:5 mixture of propylene glycol and water was atomized and fed to the intake runner of the engine head. The six-jet atomizer used generates particles with diameters in the range of 0.6 to 1.5 μm. These particles are small and light enough to follow the complex motions of the air inside the cylinder. A coincidence window of 2μs was defined as the maximum amount of time between signal recognition from each component to be considered one event.

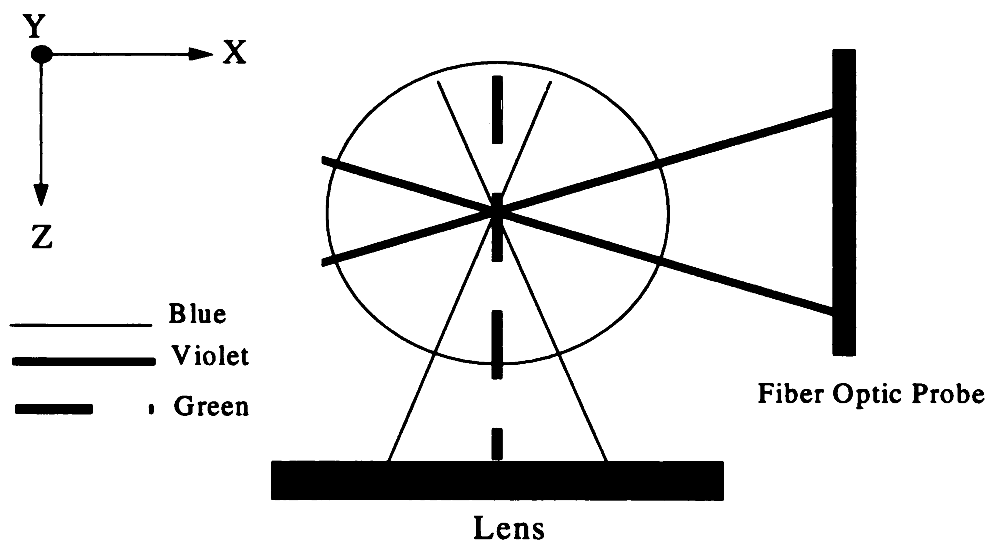


Figure 6: Beam measurement directions

The forward scattered Doppler signals were detected by photomultiplier tubes (PMT) mounted on the arms of the traverse table. The PMTs convert the received signal to an electrical signal which is sent to the frequency shifters, to adjust for the zero velocity reference signal. This signal is sent to the Digital Burst Correlator, which separates good signals from noise. The angle encoder attached to the engine head camshaft produces 1024 pulses per revolution. The resolution can be increased by a factor of 2 or 4 through the data acquisition and processing software, PHASE. The Rotating Machinery Resolver tracks the crank angle of the engine from the signal sent by the angle encoder and sends the information to the digital burst correlator. Each measurement records three components of velocity and an encoder angle so that an average velocity at each crank angle (ensemble averaged ) can be generated by the PHASE software.

# EXPERIMENTAL PROCEDURE

## MEASUREMENT LOCATIONS

Since LDV is a point measurement method and the flow field is highly variable, it is necessary to measure a large number of points to fully describe the flow. For this study 2 planes of data were taken for each configuration, each plane consisting of a 12 x 17 grid with 5 mm spacing (Figure 7). A total of 204 points were measured for each plane, with the center column of each plane overlapping the other plane. Measurements were not taken closer to the cylinder walls because the curvature of the quartz cylinder either

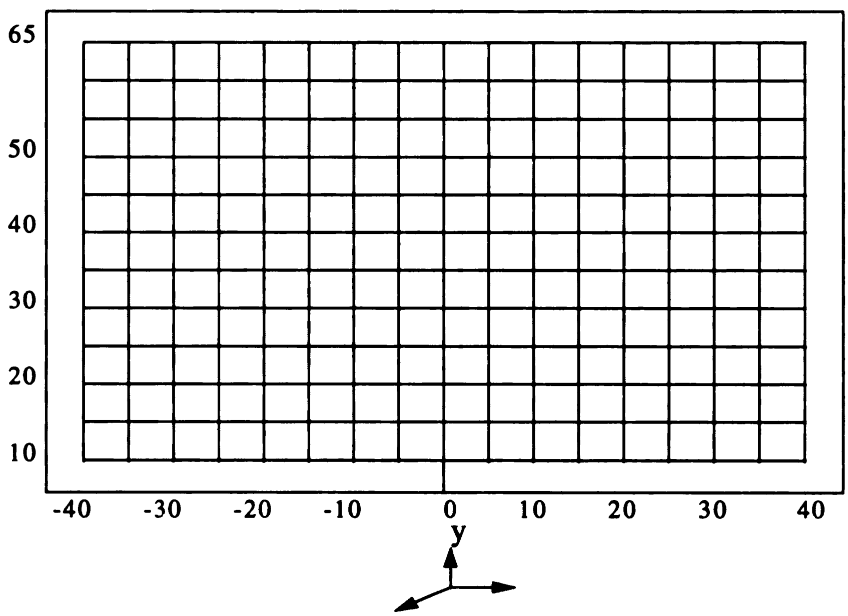


Figure 7: Measurement Grid

prevented the beams from crossing or created reflections which blocked out the signal to the photodetectors. Measurements could not consistently be taken higher than 65 mm because of the physical obstruction of the photodetectors' line of sight by the piston and the engine head.

The two planes measured are shown in Figure 8. Plane 1 is the y-z plane, bisecting the cylinder and separating intake-exhaust pairs. Plane 2 is perpendicular to Plane 1, on the x-y plane. Plane 2 bisects the cylinder, separating the exhaust valves from the intake valves. The data points on Plane 1 at z= 0 are the same as Plane 2 at x=0. The origin of

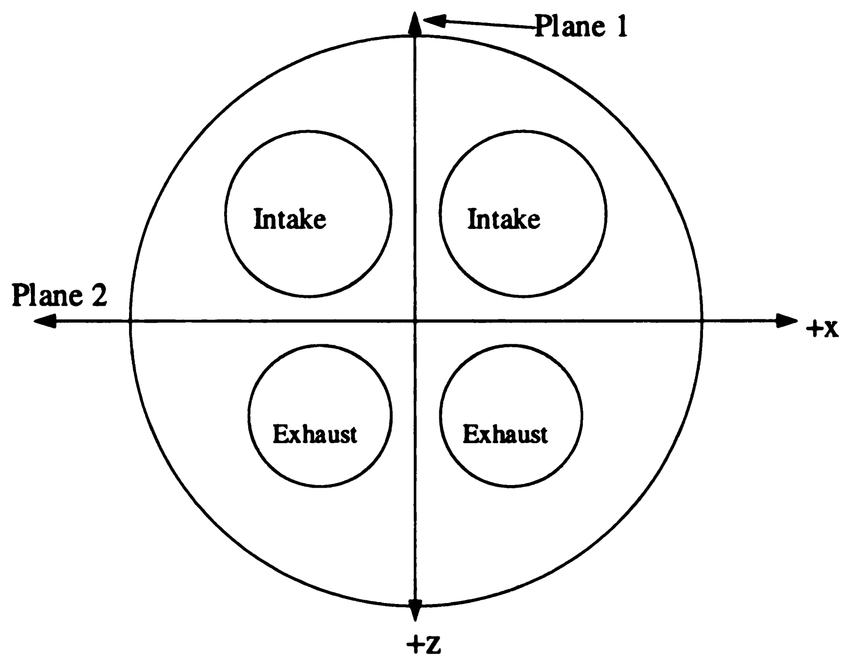


Figure 8: Measurement Plane Locations

the coordinate system was taken as the center of the piston face, at bottom dead center (BDC, the lowest position of the piston). The y axis runs along the axis of the cylinder, the positive z direction points into the laser source for the green and blue beams, and the positive x direction points into the source of the violet beams.

## DATA PROCESSING

A detailed log of position, frequency shift magnitude and direction, and other pertinent configuration information was kept while measurements were taken. This information was entered into a database. A FORTRAN program, COMPARE.FOR was created to read in velocity files generated by the LDV software, PHASE, and compare its set-up data with the database, to detect any errors in operation of the equipment. If all the information matched, the program read the velocity files, and created a new file for each measurement point consisting of the three components of velocity and their standard deviations and turbulence intensity at specific crank angles.

The velocity files were transferred to a Silicon Graphics Indigo II workstation, and were used as the data for an EXPLORER program created by ERL staff to create 3-D images of the flow fields. Using the Movie Maker utility, these images were combined into an animation of the flow field. FORTRAN programs were created to generate vorticity, circulation, turbulent kinetic energy, tumble and swirl data. This data was arranged and made into graphs using Microsoft Excel.

## CALCULATIONS

All data generation was done on a plane by plane basis. Vorticity, circulation, and tumble calculations were therefore restricted to use of certain components for their calculation. Vorticity is defined as

$$\overline{\omega} = \nabla \times \overline{V} \qquad (1)$$

For Plane 1 (y-z plane) only the *i* component of vorticity was used

$$\overline{\omega}_x = \left( \frac{\partial w}{\partial y} - \frac{\partial v}{\partial z} \right) \tag{2}$$

Similarly, for Plane 2 (x-y plane) only the *k* component of vorticity was used

$$\overline{\omega}_z = \left( \frac{\partial v}{\partial x} - \frac{\partial u}{\partial y} \right) \tag{3}$$

Three-point or five-point numerical derivatives were used to calculate vorticity at each grid point.

Circulation is defined as the integral of vorticity:

$$\Gamma = \int_A \overline{\omega} \bullet \hat{n}\, dA \tag{4}$$

Three different circulation numbers were generated: average circulation, RMS circulation, and total circulation. First the average vorticity of the 4 points making a grid cell, times the area of the cell, is calculated.

$$\gamma = \sum \frac{\omega}{4} * (5 / 1000)^2 \tag{5}$$

Total circulation is the standard completion of the numerical circulation calculation

$$\Gamma_t = \sum \gamma \qquad (6)$$

Average circulation divides the total circulation by the number of points used in the calculation. This removes variations due to the number of data points used.

$$\Gamma_a = \frac{\Sigma\gamma}{n} \qquad (7)$$

RMS circulation was generated to observe the magnitude of circulation alone, removing the canceling effect of vortices in opposing directions

$$\Gamma_r = \sqrt{\frac{\Sigma\gamma^2}{n}} \qquad (8)$$

The LDV data was also used to generate Tumble and Swirl numbers for the heads tested. Tumble and swirl calculations were based upon equations developed by GM Research Lab in SAE paper #900257 [1]. These equations were developed to use data generated by computer simulations of in-cylinder flows during intake and compression. The equations produce tumble and swirl numbers at each crank angle, rather than an overall number for the whole cylinder/head/piston setup, which is the current industry practice. The tumble number about each axis can then be plotted against crank angle, and different setups can be compared during intake, during compression or across the whole cycle.

The following equations were used as the basis for developing tumble and swirl calculations from LDV data. Normalized swirl and tumble ($T_b$ ) were defined as mean angular momentum ($H_b$) about an axis divided by the moment of inertia ($M_b$) about the same axis, normalized by the crankshaft speed.:

$$H_b = \int_{V(t)} \langle \rho \rangle \mathbf{r} \times \hat{\mathbf{U}} \bullet \mathbf{b} \, d\tau \tag{9}$$

$$M_b = \int_{V(t)} \langle \rho \rangle \left| \mathbf{r} \times \mathbf{b} \right|^2 d\tau \tag{10}$$

$$T_b = \frac{60 H_b}{2\pi M_b \Omega_{cs}} \tag{11}$$

where <ρ> is the average density, **r** is the position vector from a point to the origin, $\hat{\mathbf{U}}$ is the density weighted average velocity, **b** the unit vector of the chosen axis, and $\mathbf{\Omega}_{CS}$ the crankshaft speed. Swirl is defined as the tumble ratio ($T_b$) about the axis of the cylinder (the y axis in this project).

With LDV, a finite number of point measurements are made. The integrals above were therefore converted to summations. The vector equations were broken down into components (x, y, z being components of **r** and u, v, w being velocity components). The equations were further reduced because the density of the charge at any location was unknown. Assuming constant density at any given crank angle, constant measurement volumes of $(5\text{ mm})^3$, and constant crankshaft speed of 600 rpm, the tumble numbers reduce to:

$$T_x = \frac{\sum(yw - zv)}{\sum(z^2 + y^2)}\frac{1}{20\pi} \tag{12}$$

$$T_y = Sy = \frac{\sum(zu - xw)}{\sum(x^2 + z^2)}\frac{1}{20\pi} \tag{13}$$

$$T_z = \frac{\sum(xv - yu)}{\sum(y^2 + x^2)}\frac{1}{20\pi} \tag{14}$$

Two origins were used for the tumble calculations, based on those used in the GM study. The first was the center of the piston face at top dead center (TDC: x = 0.0 mm, y = 80.0 mm, z= 0.0 mm). The second was a moving origin positioned at the center of the cylinder volume at any given crank angle. (x = z = 0.0 mm, y = (chamber height - piston height)/2 ). The GM study based their moving origin on the instantaneous center of mass of the charge. The center of the volume was chosen as the best approximation.

## RESULTS & DISCUSSION

Appendix A contains printouts of the flow visualization results. Configurations M and N are presented side-by-side at the same crank angle for each plane. Appendix B shows views of planes 1 and 2 from the side and top to help show why the graphs of tumble ratios have their specific shapes

Plane 1 has the most organized flow in configuration M. As early as $80^o$ the beginnings of a counter clockwise rotating vortex can be seen. By $90^o$ two primary flow regions can be seen developing: one on the +Z side of the cylinder forming the vortex, and one going down the side of the cylinder on the -Z side. As the cycle advances, the region of flow circling the vortex increases, and the vortex moves upwards. The flow going down the cylinder wall decreases gradually, overpowered by the opposing flow and totally reverses by $190^o$ . As compression continues, the vortex center continues to move upwards and to the right ( -Z direction), out of the measuring region.

The flow visualization for configuration N, plane 1 has similarities to configuration M. The strong burst across the top of the cylinder creates a jet down the left (+Z) side that forms a counter-clockwise vortex as it impinges on the piston. Unlike M, a similar burst occurs on the right (-Z) side, creating a clockwise vortex. This new formation is due to the unblocked port that M did not have. By the end of intake ($180^o$) the clockwise vortex is broken down, and the entire flow field is in a counter-clockwise direction. As compression continues the center of rotation moves upward and out of the measured area.

The compression flow is similar to that of configuration M, but of lower velocity, due to the opposing jets during intake.

Both configurations show flow along the face of the pistons during intake, and flow away form the piston during compression. Taken in the context of the entire flow visualization, these piston effects do not appear to cause major variations form the existing flow patterns (beyond the reduction of volume). The different vector sizes and directions match with the flow patterns developed in the region away from the piston due to intake configuration. Previous studies at the MSU ERL showed obvious interaction between the flow and large pop-ups [2, 3].

The flow pattern of configuration M, plane 2 is harder to visualize since the entering flow is primarily perpendicular to the plane, entering the measuring region after curving off the cylinder walls or piston head. At a crank angle of $110^{o}$ a circulating region in the lower left (-X) side begins to develop, while the right side begins to develop a flow that curls to the right and upward, while the lower center region goes strongly into the page (-Z). At the end of intake, both wall flows have taken on a strong upward and leftward pattern, with traces of the circulating region remaining near the left cylinder wall. The center flow decreases in strength, but continues into the page. As compression begins, the flow starts to take on a stronger upward path. By $260^{o}$ the downward flow of the left side and the rightward flow along the piston face have been negated or moved out of the measuring area. The final images show predominantly upward flow.

During intake, plane 2 of configuration N has three distinct regions: left, right, and center. The left and right side develop small vortices at the piston, created by a downward flow along the cylinder wall with an upward flow on the inside boundary. The central region of flow is strongly into the page (-Z). By the end of intake, the upward flow of the left and right region come together, eliminating the upper half of the central region. During compression the flow off the piston face goes upward and outward (towards the cylinder walls), while higher in the cylinder the flow curves back inward. The -Z direction of flow remains, but is greatly weakened during compression. The outward flow pattern is called squish. The piston face may be some of the cause of squish, but it also appears to be an outgrowth of the recirculation regions seen earlier in the flow visualization. The strong flow perpendicular to the plane in configuration M seems to pull the flow inward, preventing the same pattern from developing.

Figure 9 shows the average turbulent kinetic energy (TKE) at each crank angle. The average values were calculated only from non-zero values of TKE, to prevent unmeasured points from affecting the numbers. The overall shapes of the plots are very similar. The major difference is for plane 2 of configuration M, its peak value being less than half that of the other planes. Plane 1 of configuration M has the highest peak value, though not that much higher than the peaks of configuration N. Configuration M's modified inlet port apparently reduces the flow turbulence in plane 2, while the higher velocities increase the TKE in plane 1. The net effect does not increase total TKE higher than that of configuration N. Configuration N also may be more advantageous because the near equal TKE for the two planes indicate a more uniform mixing throughout the cylinder.

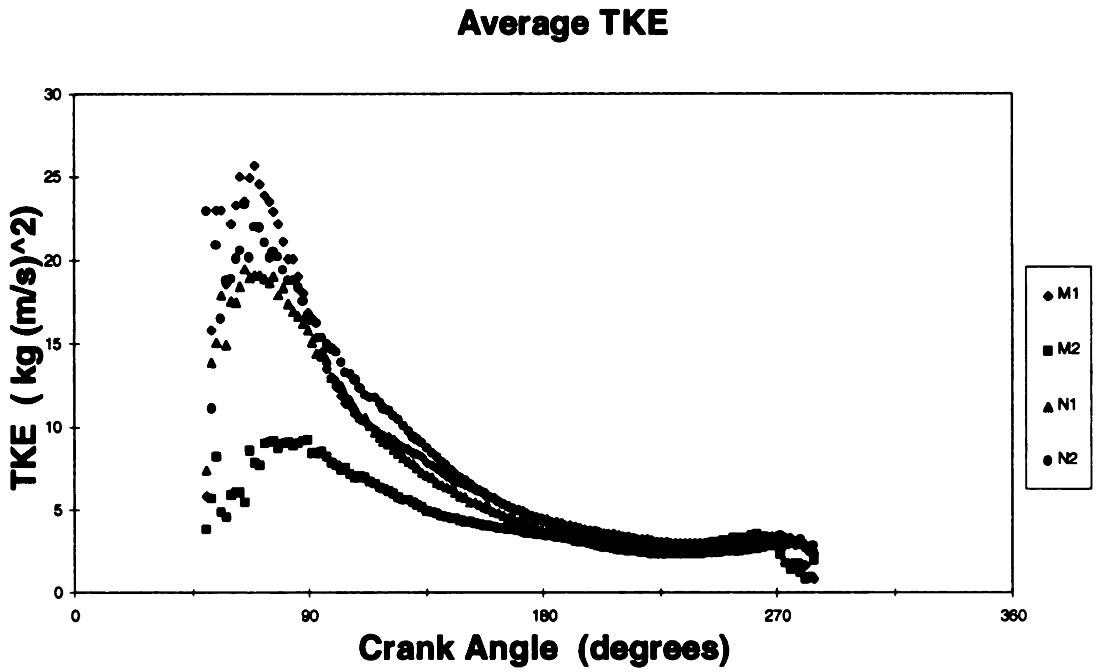


Figure 9. Average Turbulent Kinetic Energy.

As the cylinder volume increases the TKE levels for the four planes become more similar. The intake effects are reduced as flow fills the cylinder and begins circulating. During the compression stroke the values are nearly identical, with configuration M slightly higher. This may be due to the higher intake velocities from the restricted intake, or the pop-up on the piston face generating more turbulence.

The TKE values do not make a significant distinction between the four planes. The greatest differences occur during early intake, where the most differences in flow pattern appear. During compression the flow patterns have the most similarities, but are still quite distinguishable, yet TKE values are nearly identical. Therefor, the TKE values must not be greatly affected by the bulk flow patterns shown in the flow visualization..

Figures 10 to 12 are plots of the three circulation numbers versus crank angle on a plane by plane basis. Total circulation on plane 1 shows how the flow pattern differs between the two configurations. As seen in the flow visualization, configuration M has one counter-clockwise vortex that the entire flow eventually follows. This is shown in the circulation by the values all having the same sign. Configuration N contains two counter-rotating vortices, with the entire flow eventually following the counter-clockwise one. This is shown in the total circulation graph by the change in sign at about 130 degrees. The opposing directions of rotation keep the magnitude of circulation lower than that in configuration M. Configuration M's higher velocities also push the magnitude of the circulation higher on this plane. The average and RMS circulation show that for plane 1, configuration M has higher magnitudes of circulation, and that early intake has the highest magnitude of circulation. Circulation is increasing during compression, but not to the same values present during intake. This indicates that entry conditions will have a dominating effect on fuel-air mixing, since the magnitude of circulation drops off so much. More mixing will occur during compression, but not to the same extent as during intake.

In plane 2, the overall shape of the total circulation plots for M and N are similar, just shifted apart. The lower magnitudes of total and average circulation in both configurations of plane 2 , compared to plane 1, are indicative of the less organized flow seen in the flow visualizations of plane 2. RMS circulation for the two configurations are very similar to each other, and of about the same magnitude range as plane 1. This indicates the overall magnitudes of the flow in plane 2 are similar to plane 1, but disorganized so that the individual circulation cells cancel out. This condition should be better for mixing. The high RMS value indicates large amounts of circulation, while

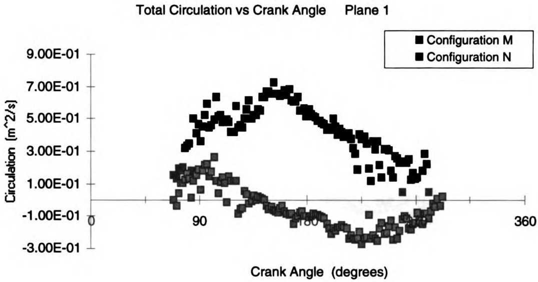


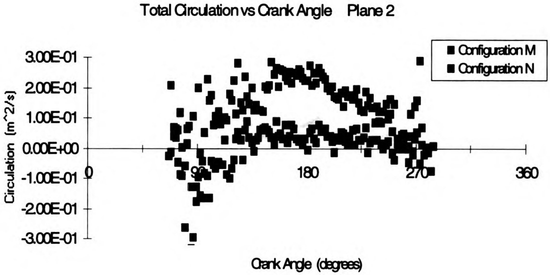


Figure 10: Total Circulation at Plane 1 & at Plane 2.

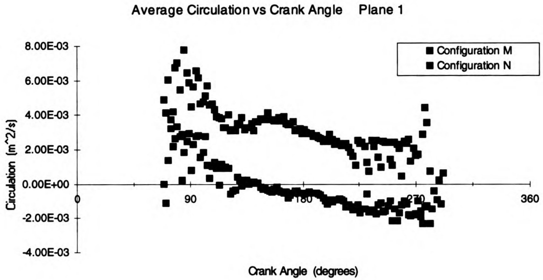


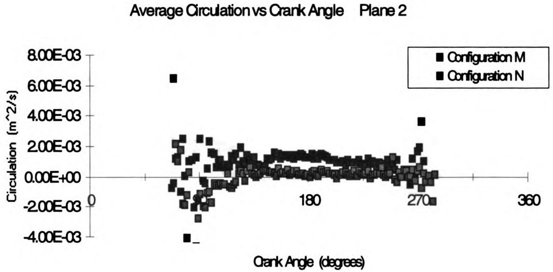


Figure 11: Average Circulation at Plane 1 & at Plane 2.

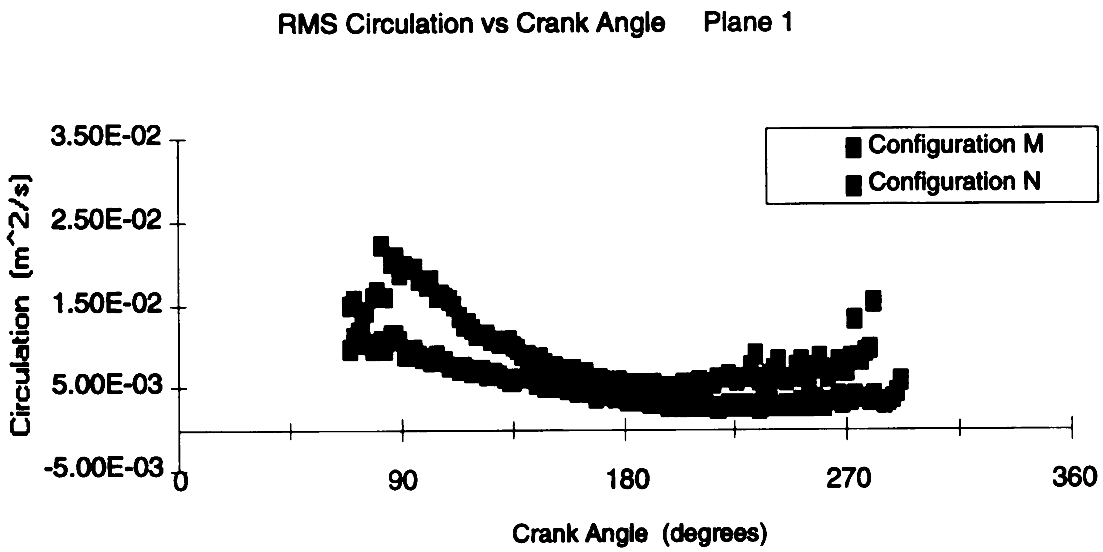


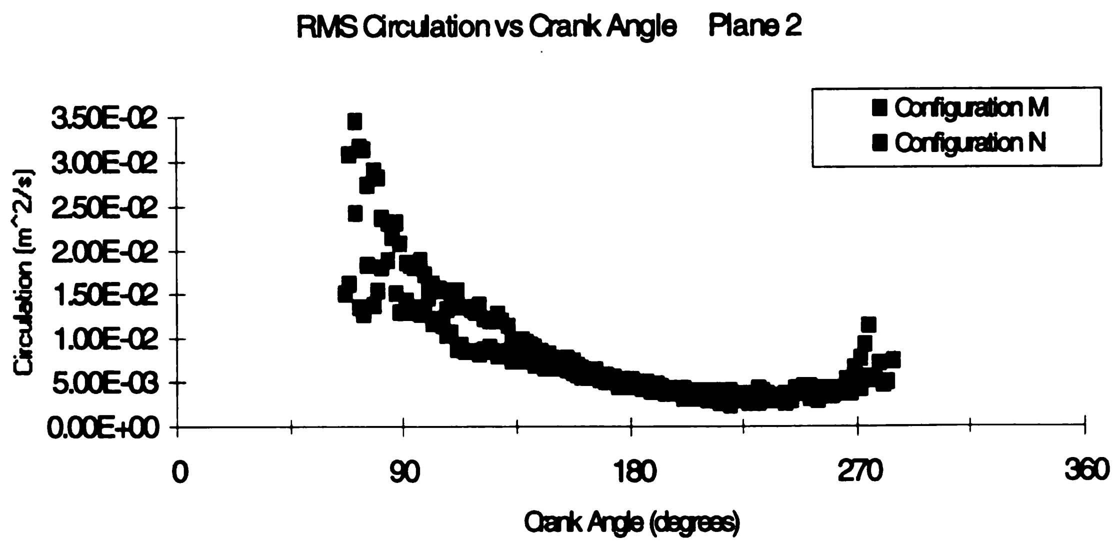


Figure 12: RMS Circulation at Plane 1 & at Plane 2.

values of Total and Average circulation near zero indicate that instead of a bulk circulation/vortex motion, the regions of circulation vary in direction canceling each other out numerically, but enhancing mixing. In plane 1 one observes a large circular motion, while in plane 2 complex smaller scale motions can be seen.

Figures 13 to 16 contain plots of tumble numbers for each plane. For all planes Y tumble is the swirl. For plane 1, X tumble is tumble about the axis perpendicular to the plane, making it the main tumble number. For plane 2, Z tumble is about the axis perpendicular to the plane. Figures are labeled either TDC Origin for the stationary origin located at the center of the piston face at top dead center or Moving Origin for the origin located at the instantaneous center of the volume in the cylinder.

For both configurations of plane 1 the X tumble follow a consistent trend: high initial value which decreases until about 270°, then slightly increasing. Configuration M's slower decrease and over-all higher values match well with the circulating flow structure and higher velocities. Configuration N's sharper decrease and lower overall values are due to opposing flow directions and lower velocities. The moving origin's values are very similar, with a minimum value corresponding to the lowest origin.

The segmentation of the data at the beginning and end of the cycle is enhanced with the moving origin, more so for the 225°-270° range. This effect is present for all of the configurations for at least one tumble ratio. This effect appears to be due to two factors. The first is the moving piston which will block or unblock nearly a whole row of points. The removal of 17 points from the calculation will cause a shift in the values. The second is the location of the moving origin. As the origin moves rows of vectors change

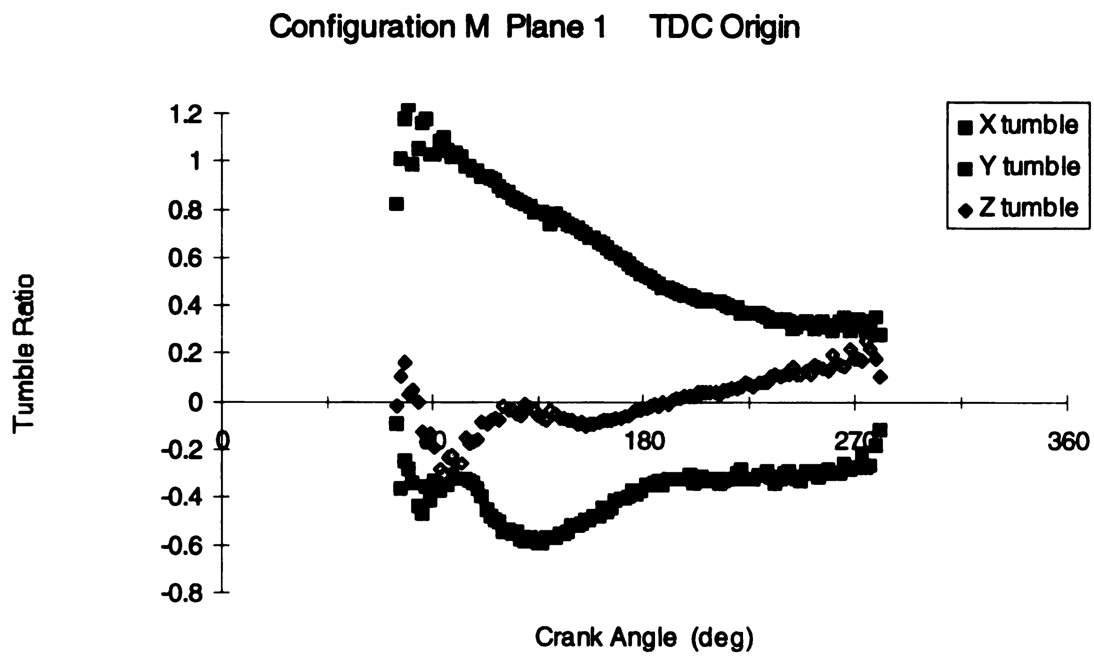


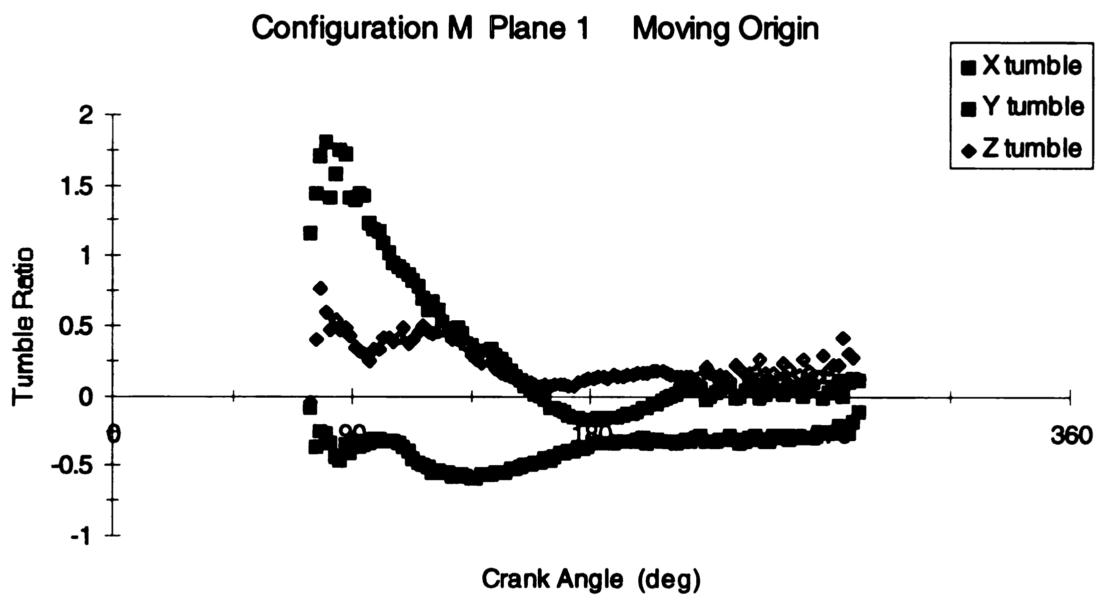


Figure 13. Tumble Ratio for Configuration M, Plane 1, TDC origin & Moving origin.

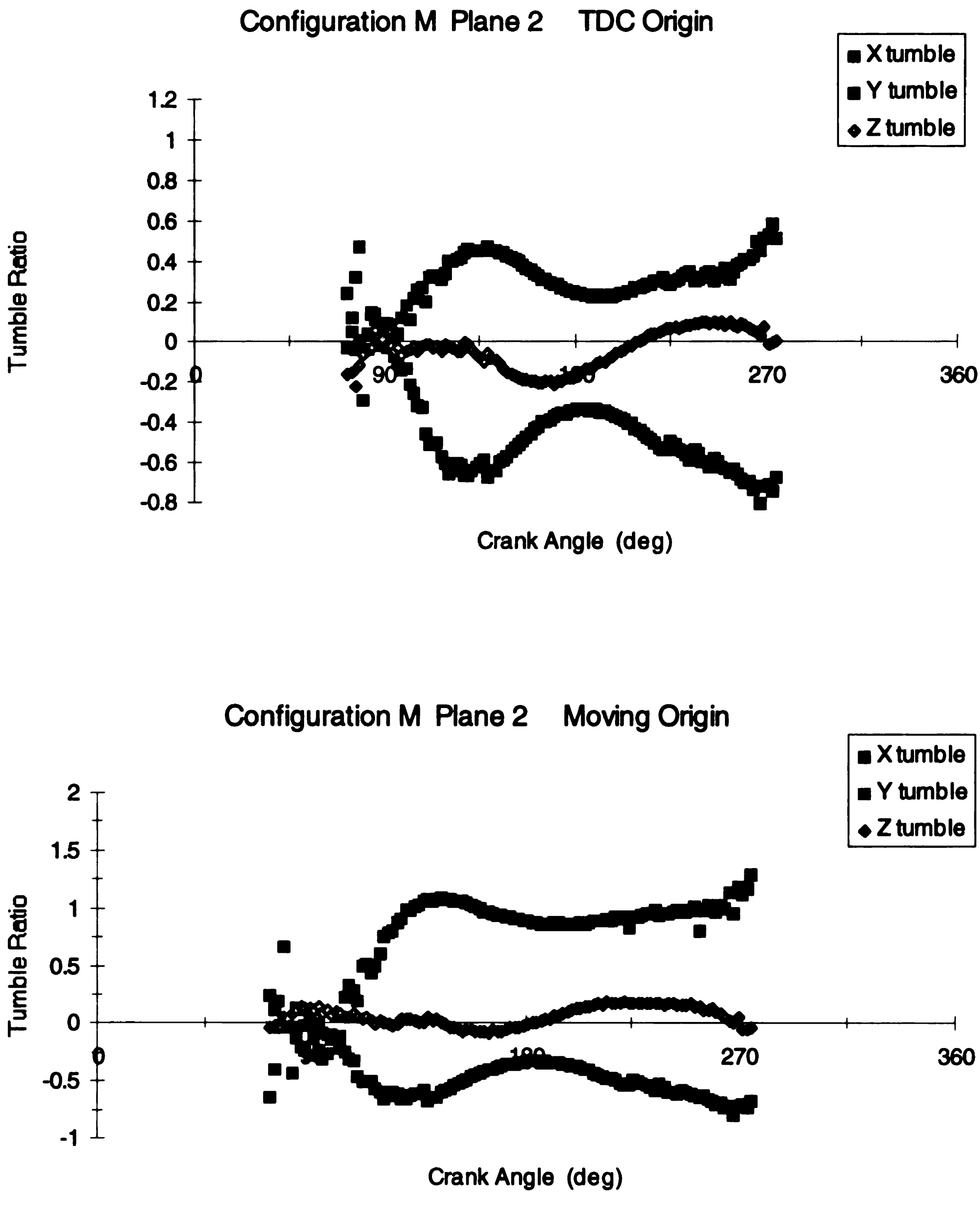


Figure 14. Tumble ratio for Configuration M, Plane 2, TDC origin & Moving origin.

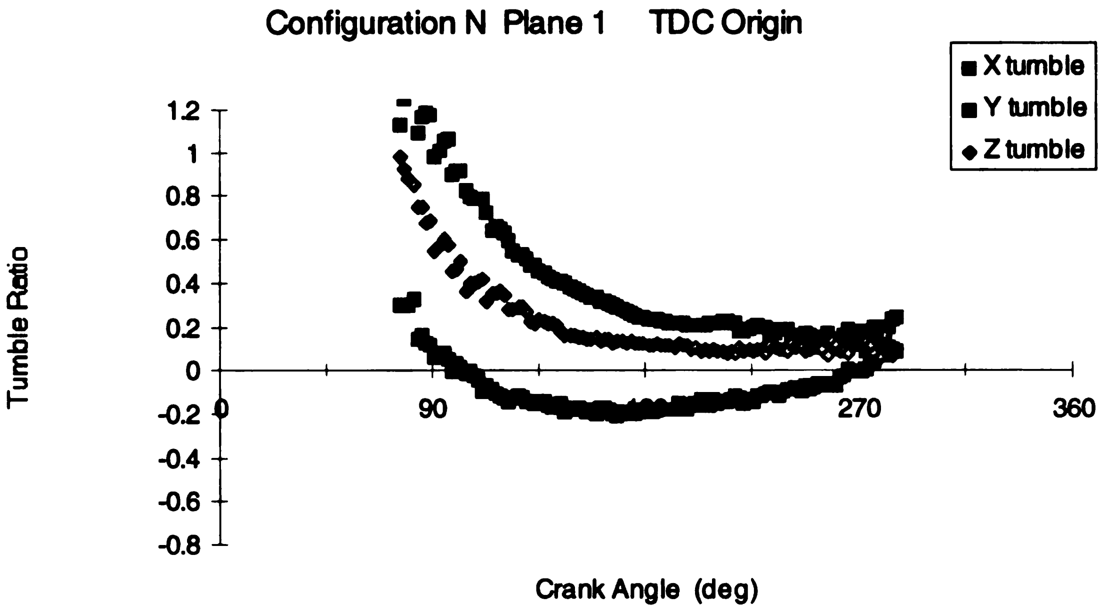


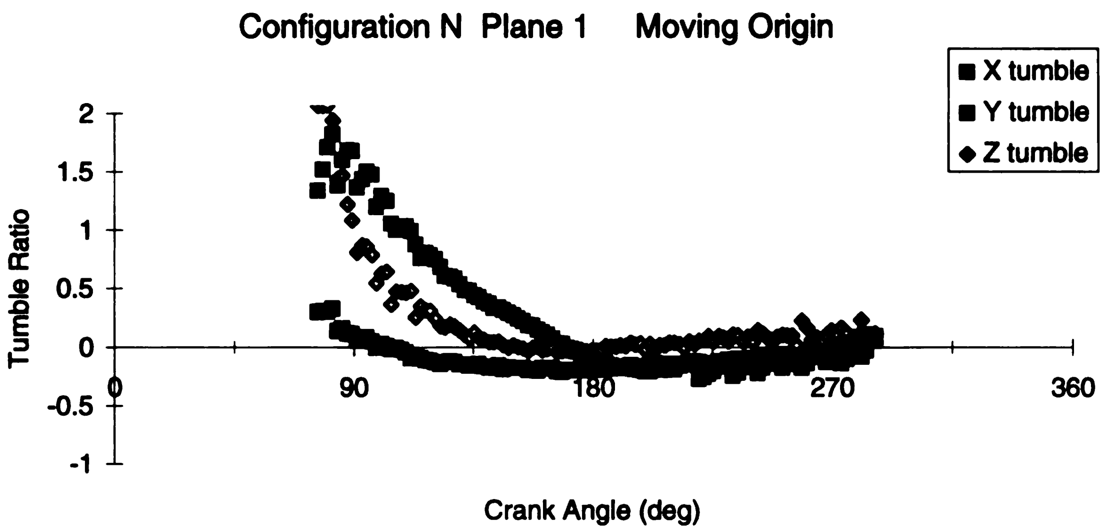


Figure 15. Tumble ration for Configuration N, Plane 1, TDC origin & Moving origin.

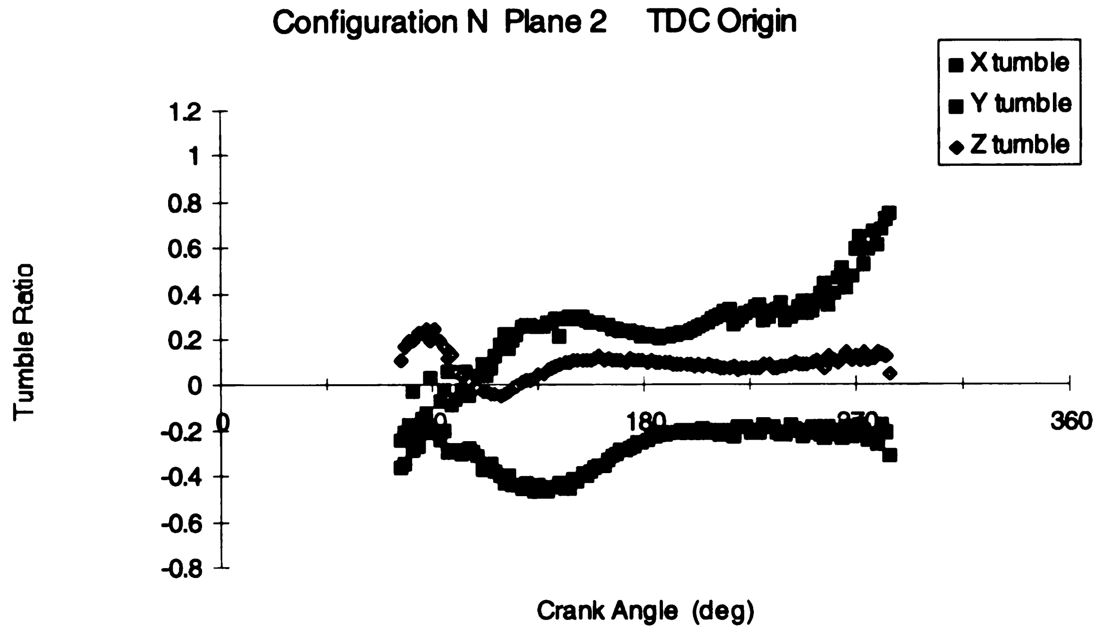


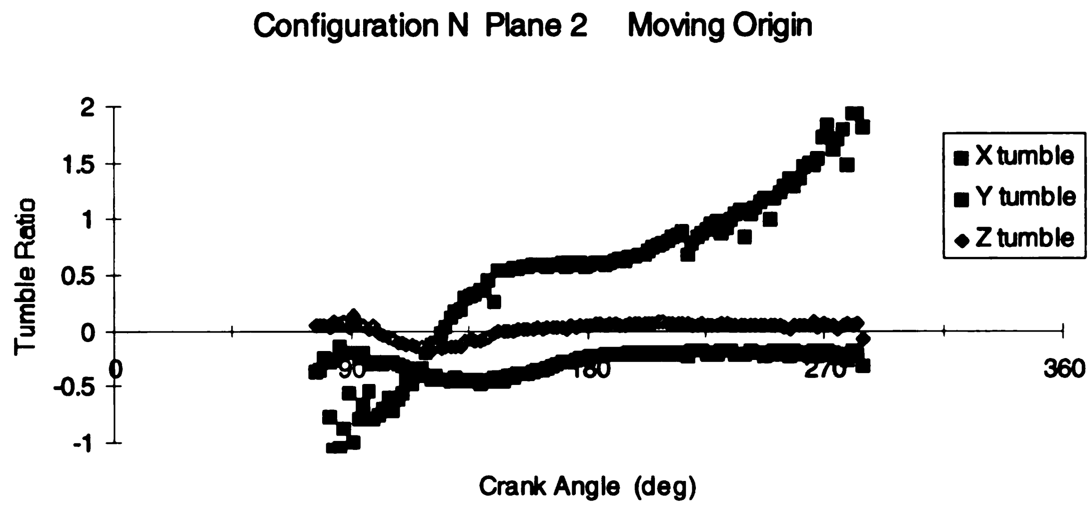


Figure 16. Tumble ratio for Configuration N, Plane 2, TDC origin and Moving origin.

from being above to below the origin, which changes the direction of rotation from clockwise to counter, or vice-versa.

The values of Y tumble for the moving origins are identical to the TDC origin values. Y tumble (swirl) for plane 1, configuration M is entirely negative, with a slight depression near 135°. For plane 1, configuration N, Y tumble has a gentle arc shape, with the ends being positive and the rest negative. Examination of the flow fields for N and M from an overhead view show how why the two are different. Figure B1 shows an overhead view of plane 1, configuration M. From 75° to 120° there are many vectors pointing perpendicular to the plane, to the left on the -Z side and to the right on the +Z side, creating a counter-clockwise moment. Figure B1 (a) shows a sample of this flow pattern at 119°. This pattern fades, leading to a reduction in tumble magnitude. The smaller magnitudes and the directions of the vectors in Figure B1 (b) exemplify this lower tumble regime. For N, the vectors are primarily along the plane, none pointing perpendicular to the plane. No discernible pattern is evident, the vectors just point in many directions. Figure B2 shows how the vectors at different crank angles are oriented so that low Y tumble numbers exist throughout the cycle.

For configuration M, Z tumble has about the same shape for the TDC and moving origins, but the slope of the entire line changes slightly. For configuration N, Z tumble for the TDC origin is similar in shape to X tumble, while Z tumble for the moving origin drops suddenly and then hovers around zero. Figures B3 and B4 show plane 1 from the side. For the TDC origin, the origin is located above the column of vectors, off the page. The vectors for both configurations appear well jumbled from this viewpoint, which matches with the tumble values near zero the majority of the time. For configuration M the difference caused by the moving origin can be understood by examining Figure B3. As the moving origin moves into the measurement area, the vectors at the top of Figure B3 (a) are now above the origin, creating a moment in the direction opposite that of the TDC origin situation. For Figure B3 (b), the vectors are going in both perpendicular directions, so that the moving origin makes less of a difference at this crank angle. For configuration N, the very steady X tumble values are due to the very planar nature of the flow. Figure B4 shows how during intake and compression the vectors are primarily parallel to the plane. This keeps the tumble magnitudes very low.

The tumble ratios for plane 2 were very similar for both configurations and origins. X tumble increases greatly, dips, and rises again. Y tumble (swirl) has a dip around 135° with a drop at 270°. Z tumble is relatively flat with a dip between 90 and 180 degrees, staying near zero. The lower tumble numbers for plane 2 ( Z tumble) vs. plane 1 (X tumble) are due to the less structured flow pattern in plane 2. The large circular motion in plane 1 produces a consistently higher number. The different regions of flow in plane 2 oppose each other, keeping the tumble ratio near zero as one region dominates then ebbs.

Figure B5 shows the overhead view of configuration M, plane 2. For early crank angles the opposing directions of the vectors seem to balance out. By 135° the +X side develops a strong flow in the -Z direction, while the opposite side has a weak flow primarily in the opposite direction (Figure B5 (a) ). This matches the low point on the Y tumble graph. As the cycle continues this pattern diminishes, gradually balancing out some, but maintaining the counter-clockwise direction of rotation. A maximum occurs at

BDC, where vectors on the +X side decrease in magnitude and more vectors point in the +Z direction (Figure B5 (b) ), opposing the counter-clockwise motion. Configuration N has a similar pattern, but to lesser magnitudes. At early and late crank angles the vectors balance each other for the most part (Figure B6 (b) ), producing steady Y tumble values. Around 135° a minimum occurs as did in M, but the vectors are smaller and less perpendicular to the plane (Figure B6 (a) ). This creates the minimum value of about -0.5 compared to -0.75 for configuration M.

For X tumble in plane 2 there is a large difference between the moving and TDC results. Viewed from the positive Z direction, the vector fields for the two planes look very similar, with minor differences in vector magnitude or direction (Figures B7 and B8). This shows in the similar X tumble numbers for the two configurations. For configuration M, the peak X tumble is achieved at 135°. Figure B7 (a) shows the many perpendicular vectors which cause the peak. The moving origin maintains higher values through the rest of the cycle because the increasing flow in the +Z direction in the upper half of the plane (Figure B7 (b) ) enhances the moment, while for the TDC origin this reduces the moment. During compression, configuration N's tumble ratios increase, more so for the Moving origin. The large increase for the Moving X tumble is due to the structure of the flow pattern. While configuration M has vectors pointing in opposing directions, N has vectors primarily in one direction near the piston and the opposing direction near the head (Figure B8 ). This creates a strong moment when the origin is in-between the piston and the top of the measurement region, as is the case with the moving origin. For the TDC origin the increase is not as large, because the opposing direction vectors cancel. This effect of the moving origin is most noticeable in this plane.

The qualitative graphical analyses above do not confirm the values of tumble, but show that the trends do follow logically from the flow field. Quantitatively, the tumble ratios calculated were within the same range as those generated in the GM report. For an unmodified 4 valve engine, they achieved numbers that were less varying and closer to zero. Many factors could account for this difference, primarily our data being planar and theirs being for the entire volume.

## CONCLUSIONS

1) Intake configuration had the dominating effect on flow patterns. The flow patterns established during intake carry through into compression.

2) The two piston top designs tested had minor affects on in-cylinder flow, mainly at the beginning of compression. Further tests with only piston head designs being changed and more measurement points near the piston face are needed to fully understand the effect of piston design.

3) The three methods of quantifying flow ( turbulent kinetic energy (TKE), circulation, and tumble) measure different types of flow motion. TKE measures variation at a measured point, circulation measures flow patterns in many small areas, and tumble measures bulk flow. Circulation and tumble values could be corroborated by flow visualization, but TKE could not. TKE makes little distinction between the four planes measured, while circulation and tumble make clear distinctions between the planes.

4) The two different origins used in the calculation of tumble ( moving and located at top dead center) can produce very different or very similar values for a given configuration. Differences in the two tumble numbers is usually indicative of a circular flow pattern.

5) To determine if any of the three quantifications is a better predictor of engine performance qualities extensive comparison of the LDV produced values with actual engine test data is needed.

6) The tumble numbers generated were within the range of values arrived at by the developers of the equations in their computations. Now that the tumble numbers have

been verified modifications and adjustments to the tumble equations can be made, such as combining individual planes data into one tumble number, normalizing tumble based on the number of points used in the calculation at each crank angle, and trying different stationary and moving origins.

# APPENDICES

# APPENDICES

Appendix A contains printouts of the velocity vector fields from each plane and configuration at seven different crank angles. Plane 1 is viewed from the +X direction, Plane 2 from the +Z direction. Configuration M is the on the left and Configuration N on the right. The pair of circles at the tip of the cylinder represent the locations of the intake valves, and are given to use as a reference point only. The images were created on a Silicon Graphics Indigo II workstation, using Explorer, and the images were formatted for print out using Showcase. Because these are three-dimensional vectors on a two-dimensional page, scaling is somewhat difficult. The thickness of the vector is the best gauge of vector magnitude, not length. The vector below is given as a scale, and is equivalent to 10m/s.

Figure 17. Vector scale: 10 m/s.

Appendix B

Appendix B contains printouts of velocity vector fields viewed from the edges of the planes, to help understand tumble numbers. For views from the +Y direction, the origin is located at the center of the line of vectors. For views from the +X or +Z directions, the origin is above the line of vectors (or starts above the line of vectors in the case of the moving origin). These figures are presented to qualitatively increase the understanding of tumble numbers. Because of the varying sizes of the planes and vectors, different scalings were used, though a consistent sizing was adhered to as much as possible.

# APPENDIX A

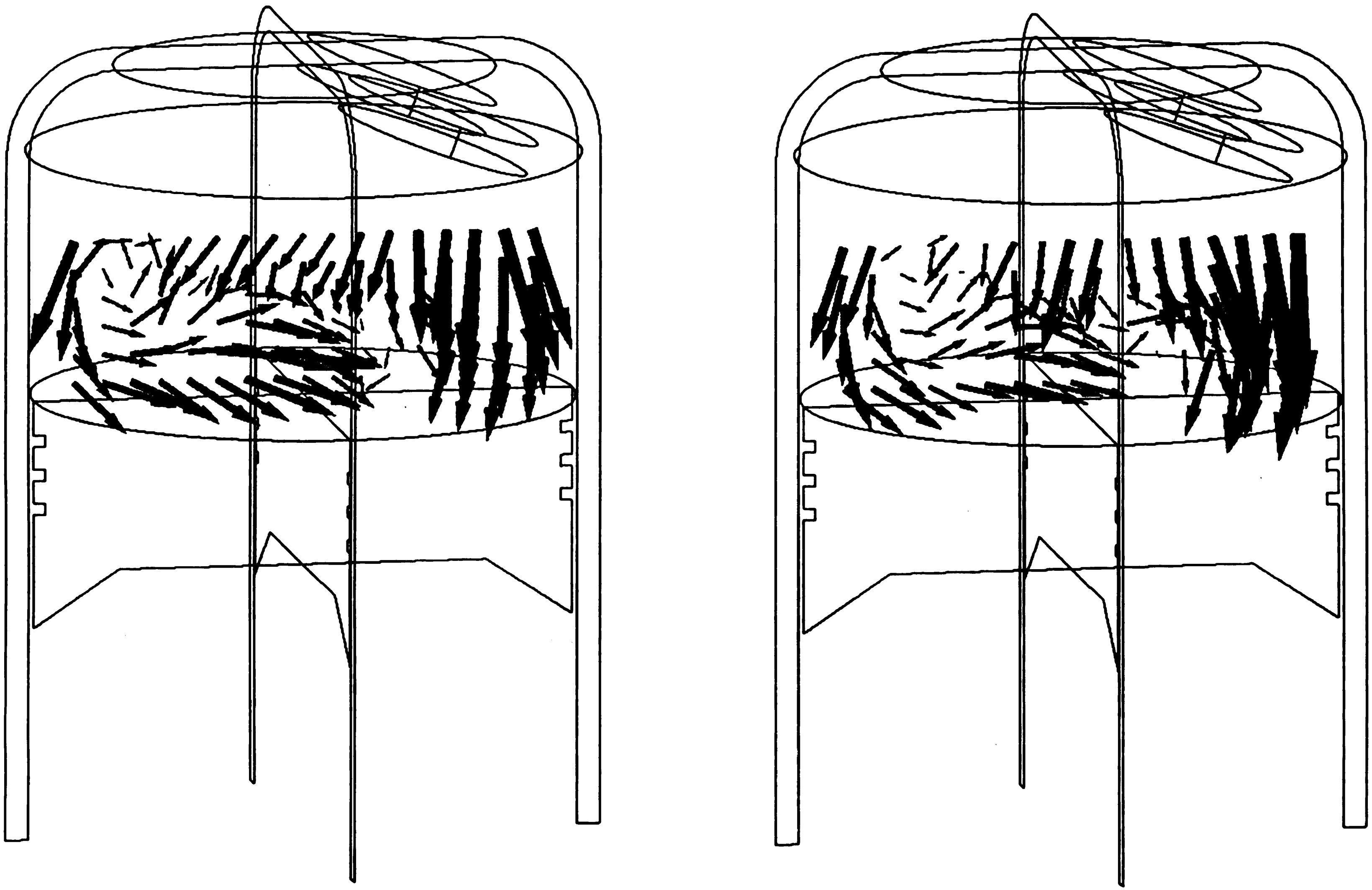

Figure A1: Vector fields for Plane 1, Configurations M and N, at 89.3 degrees.

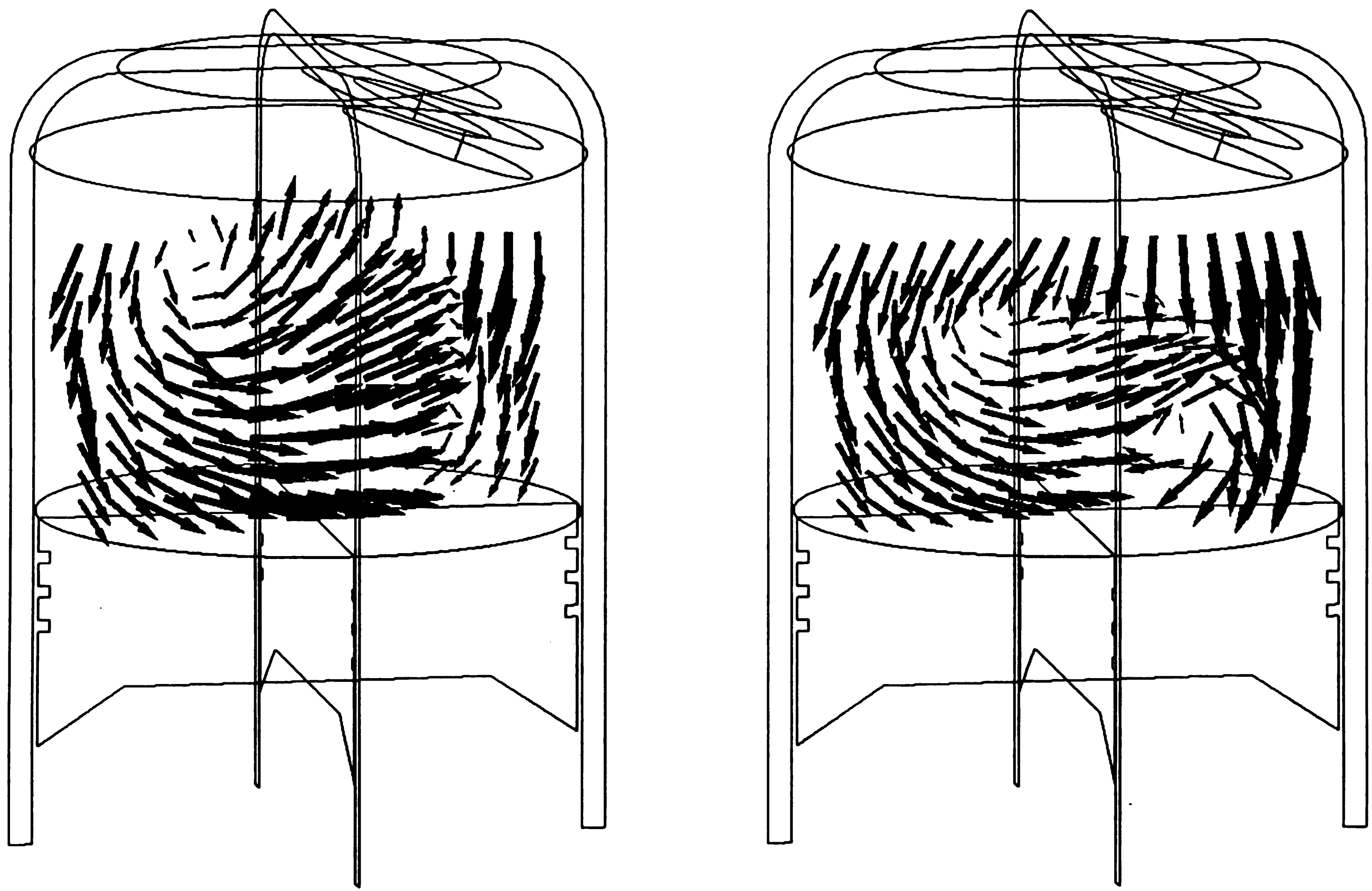

Figure A2: Vector fields for Plane 1, Configurations M and N, at 120.6 degrees.

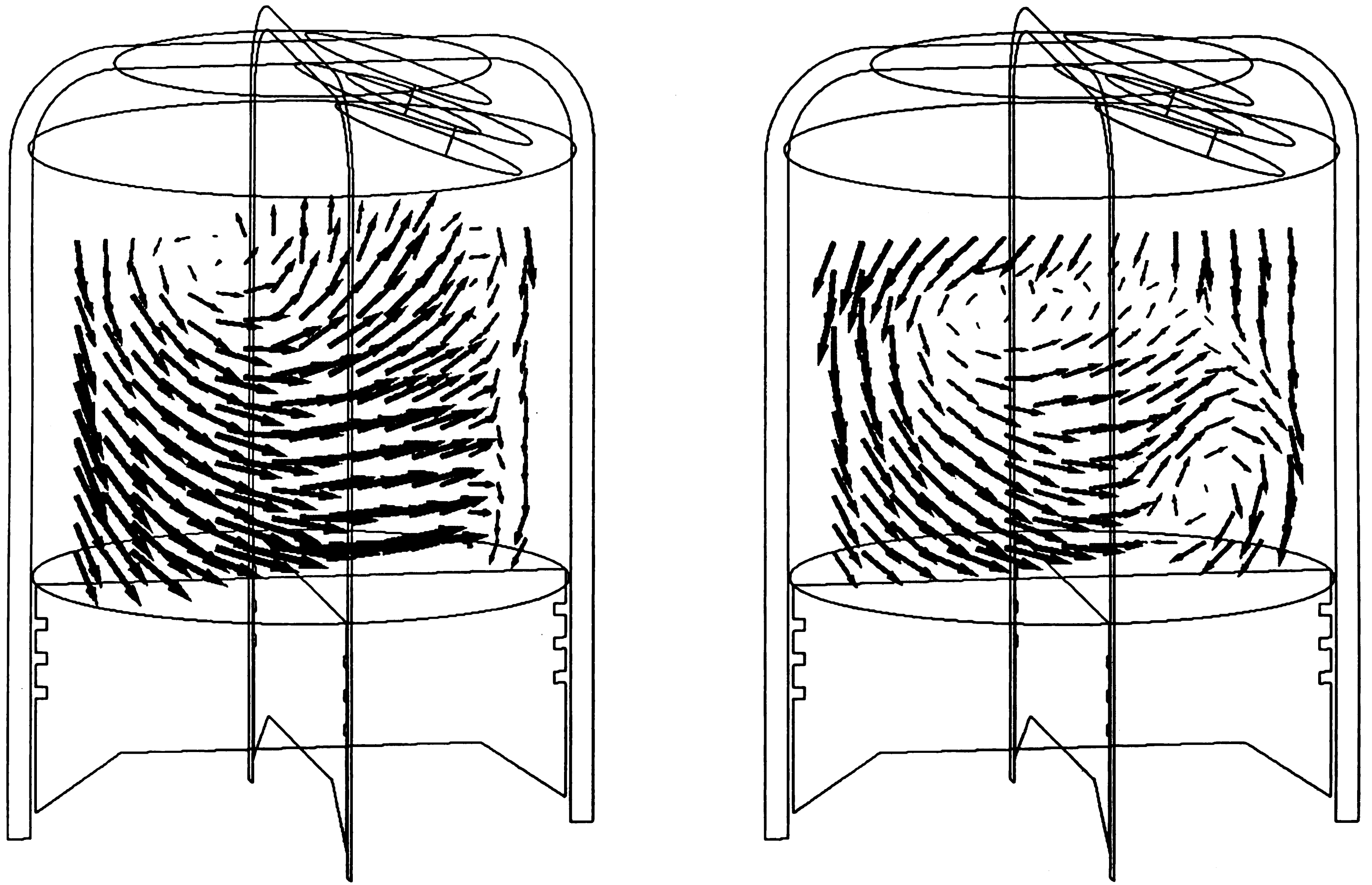

**Figure A3: Vector fields for Plane 1, Configurations M and N, at 150.1 degrees.**

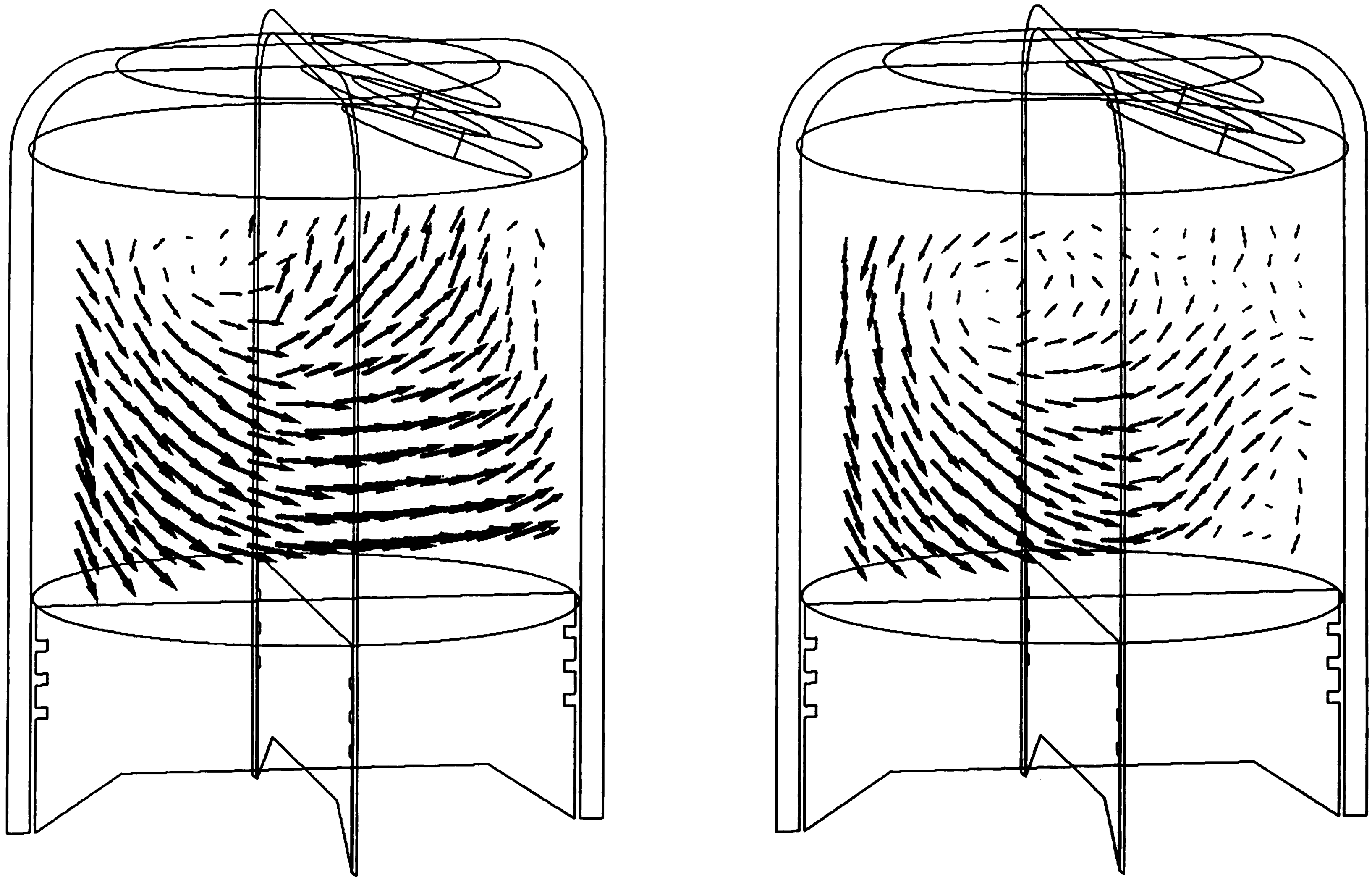

Figure A4: Vector fields for Plane 1, Configurations M and N, at 179.5 degrees.

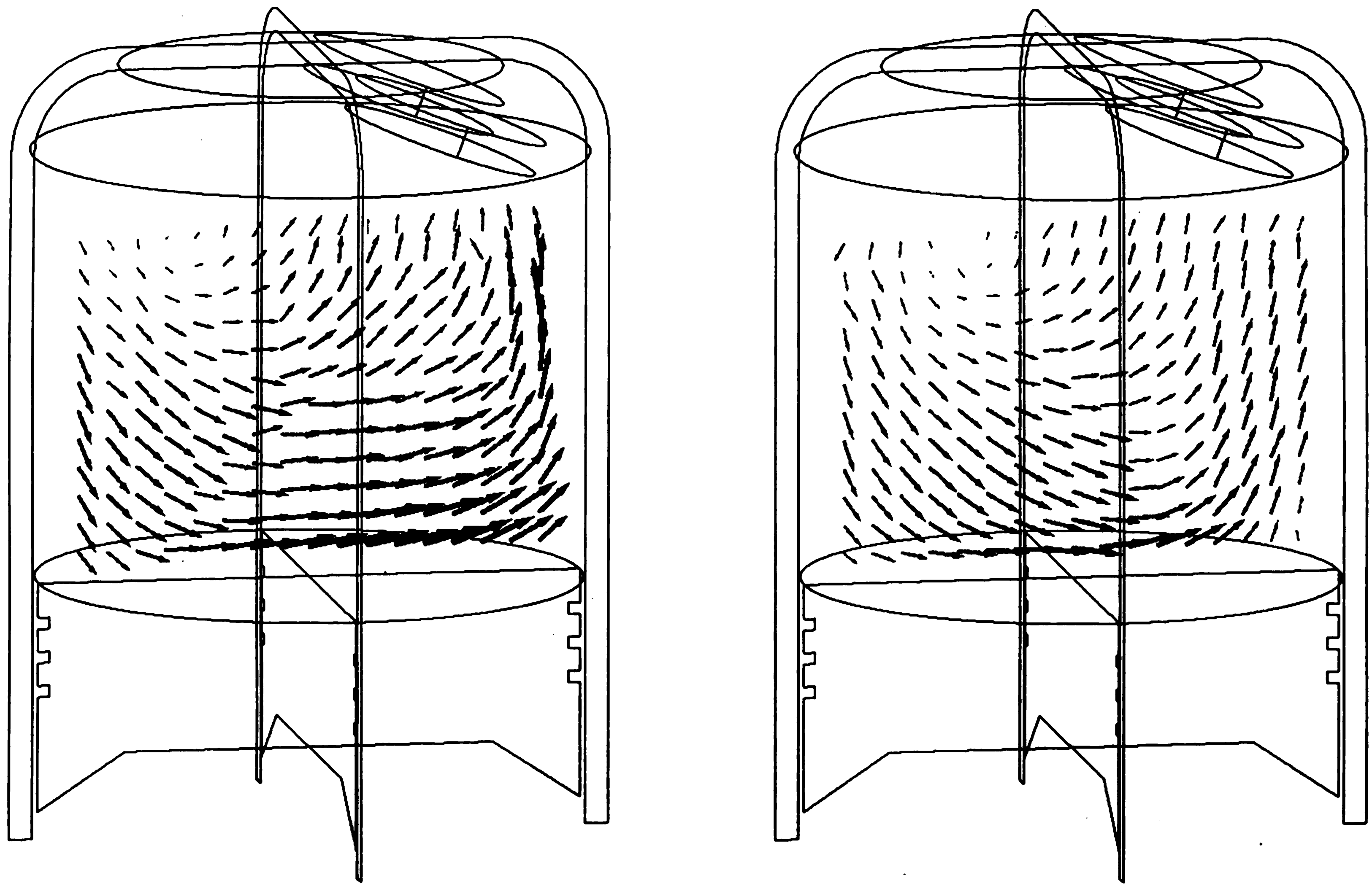

**Figure A5: Vector fields for Plane 1, Configurations M and N, at 210.8 degrees.**

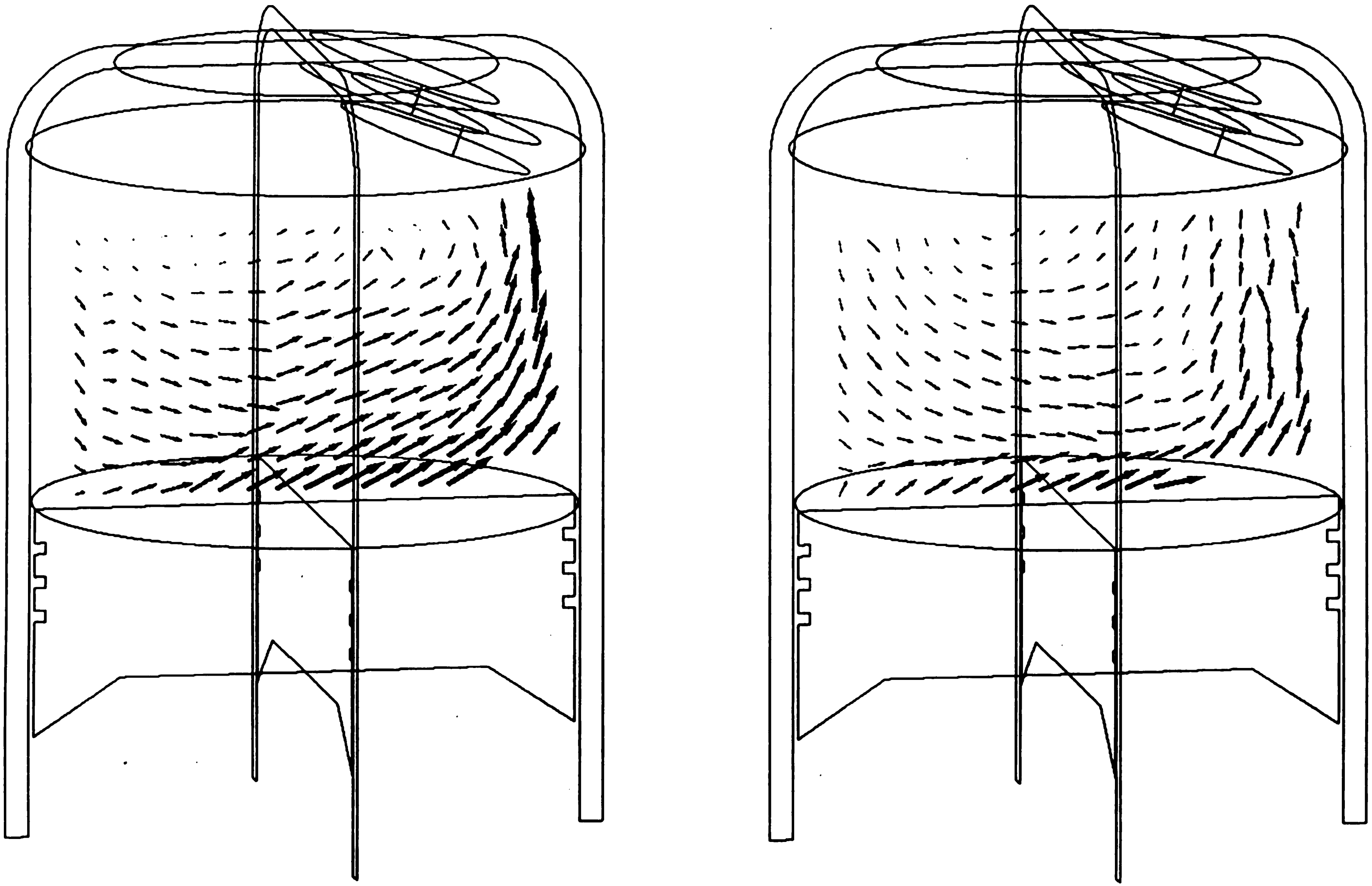

Figure A6: Vector fields for Plane 1, Configurations M and N, at 240.3 degrees.

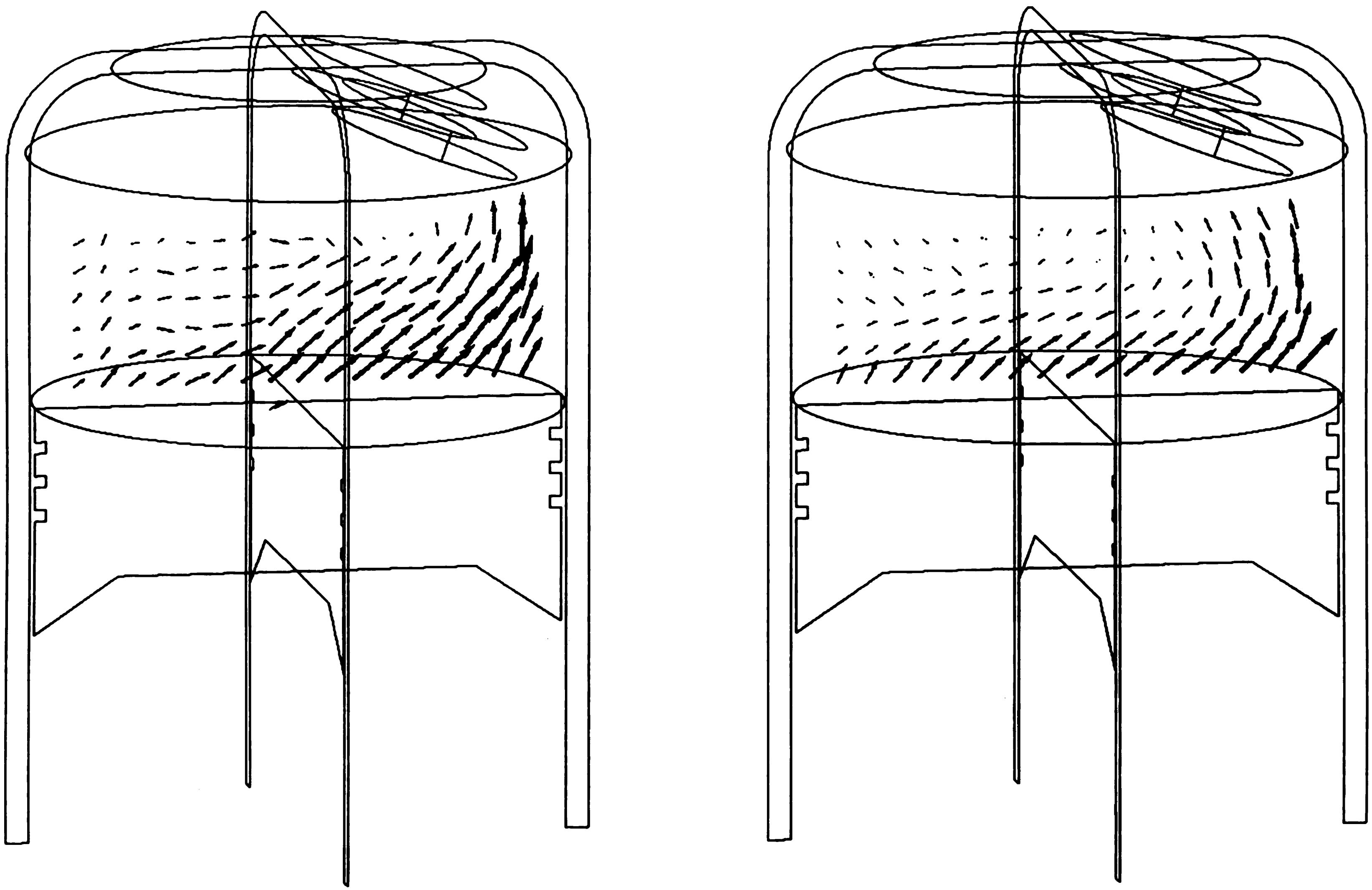

Figure A7: Vector fields for Plane 1, Configurations M and N, at 269.8 degrees.

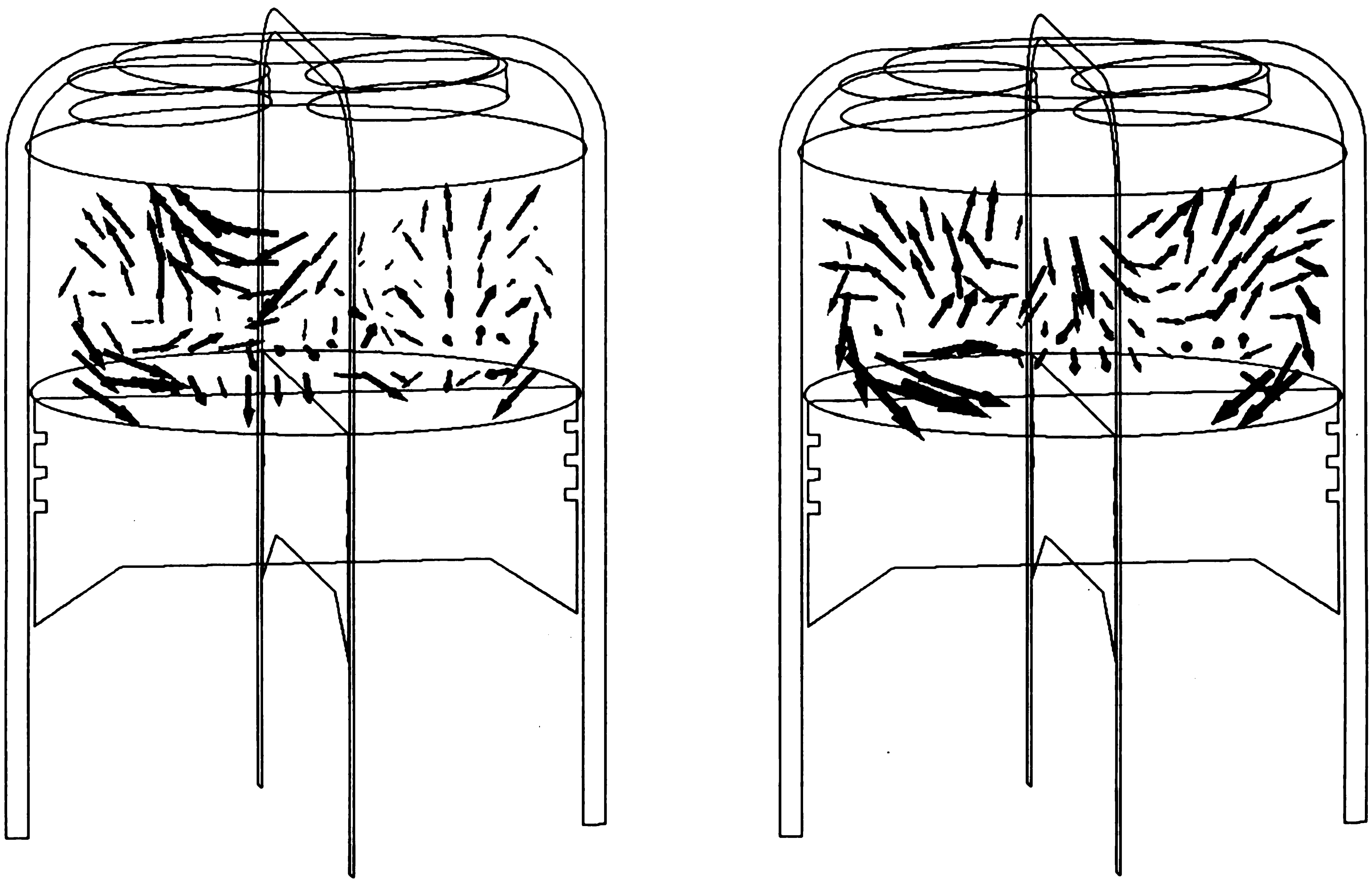

**Figure A8: Vector fields for Plane 2, Configurations M and N, at 89.3 degrees.**

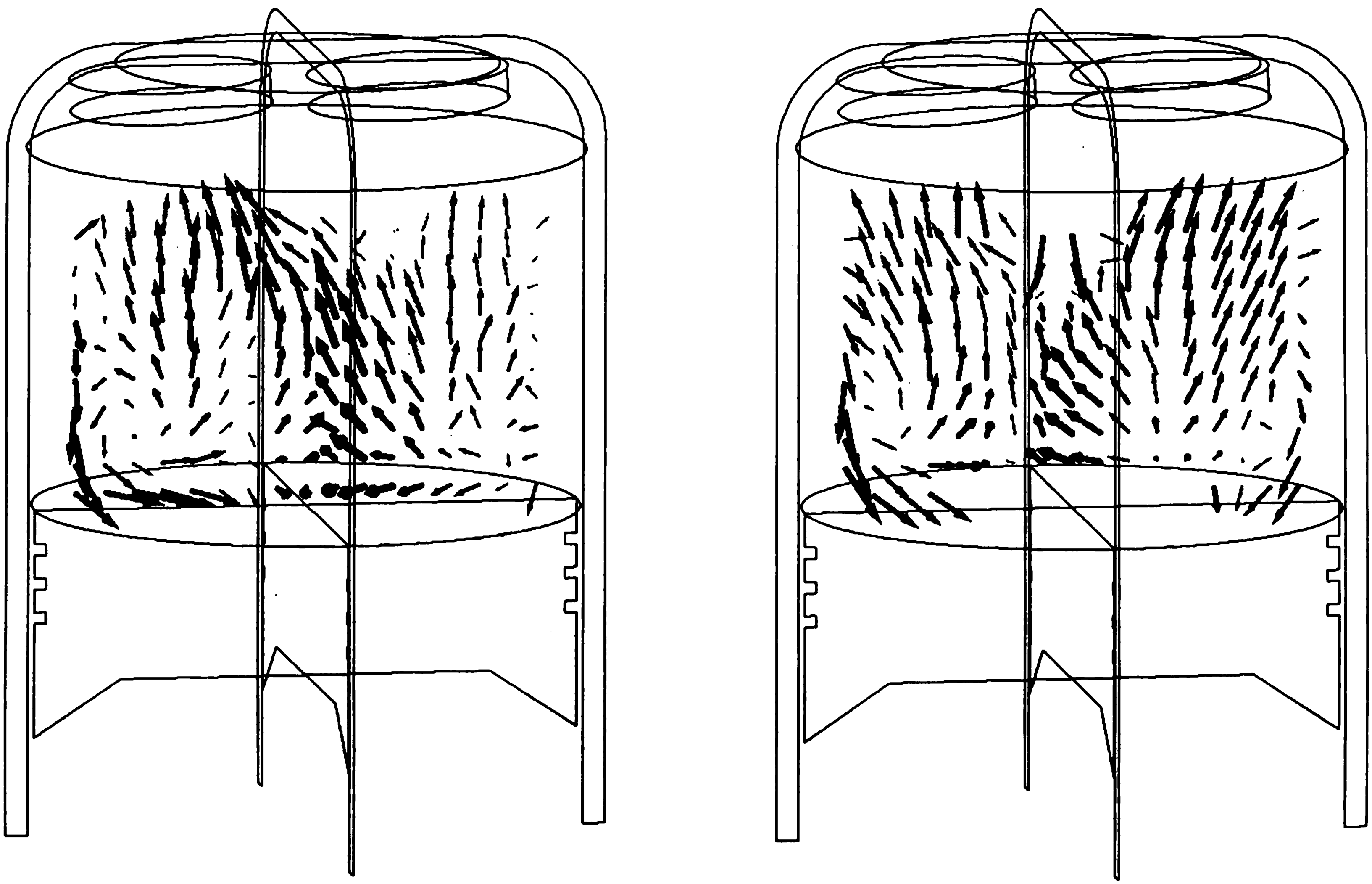

Figure A9: Vector fields for Plane 2, Configurations M and N, at 120.6 degrees.

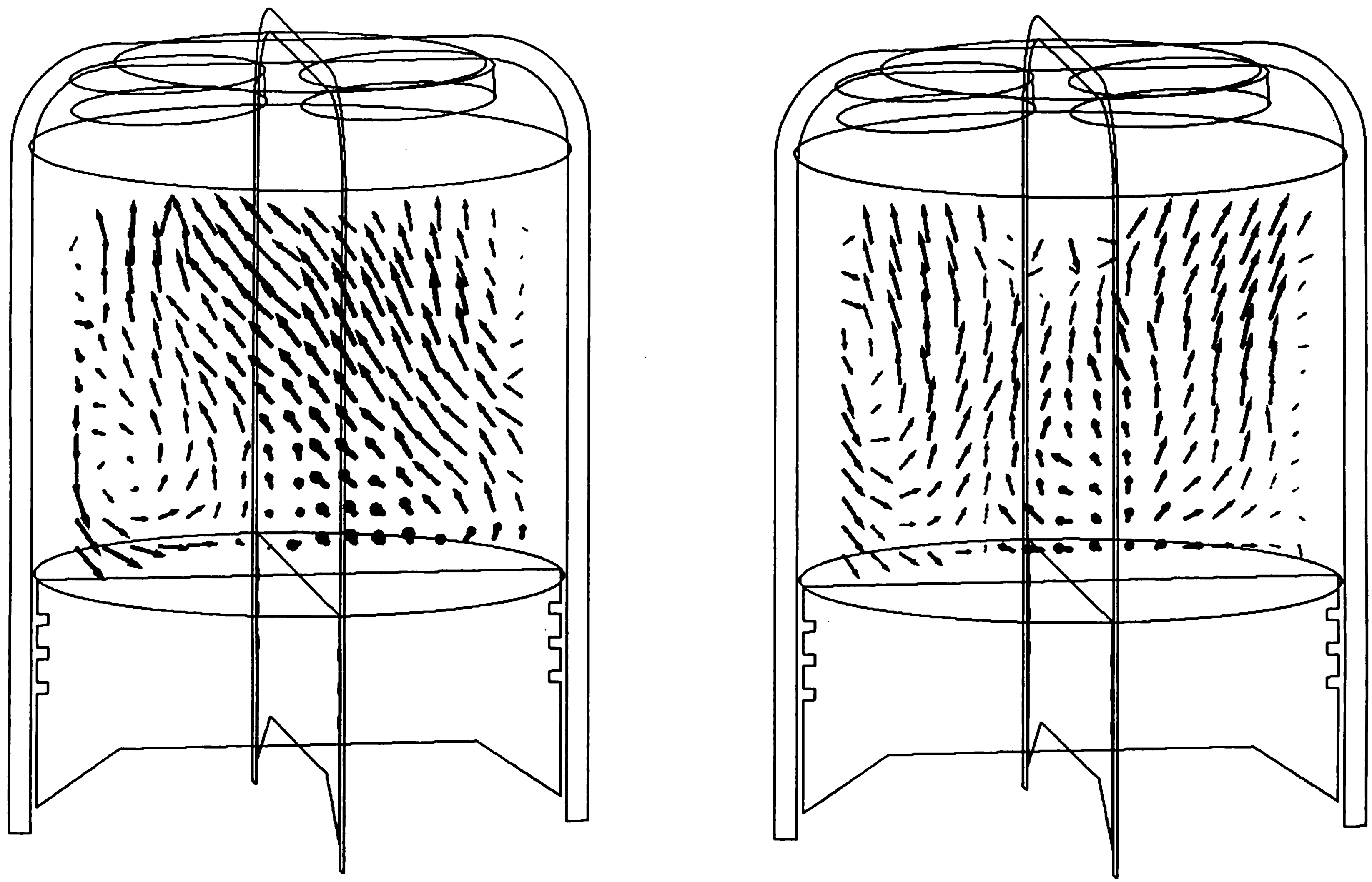

Figure A10: Vector fields for Plane 2, Configurations M and N, at 150.1 degrees.

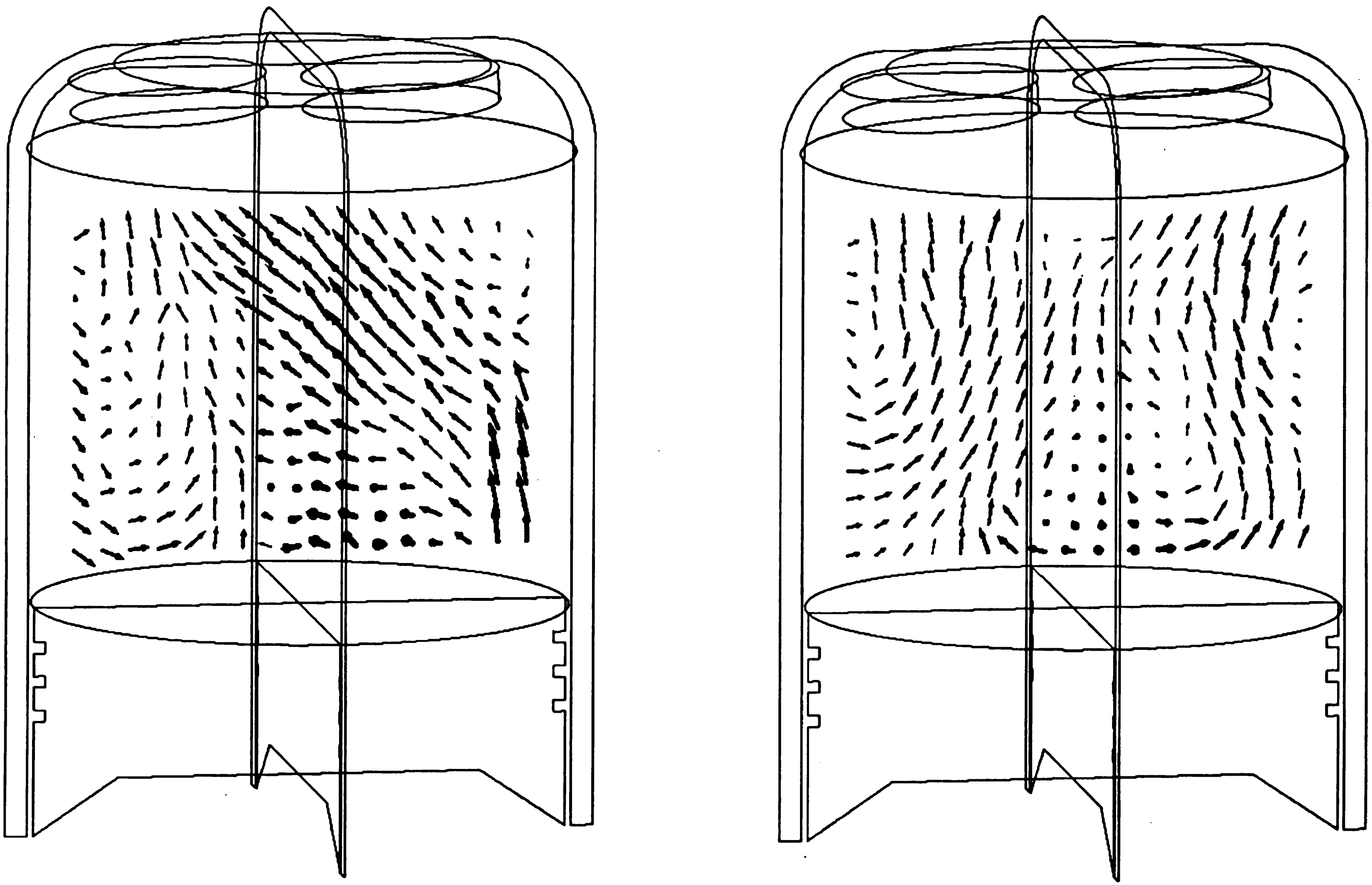

**Figure A11: Vector fields for Plane 2, Configurations M and N, at 179.5 degrees.**

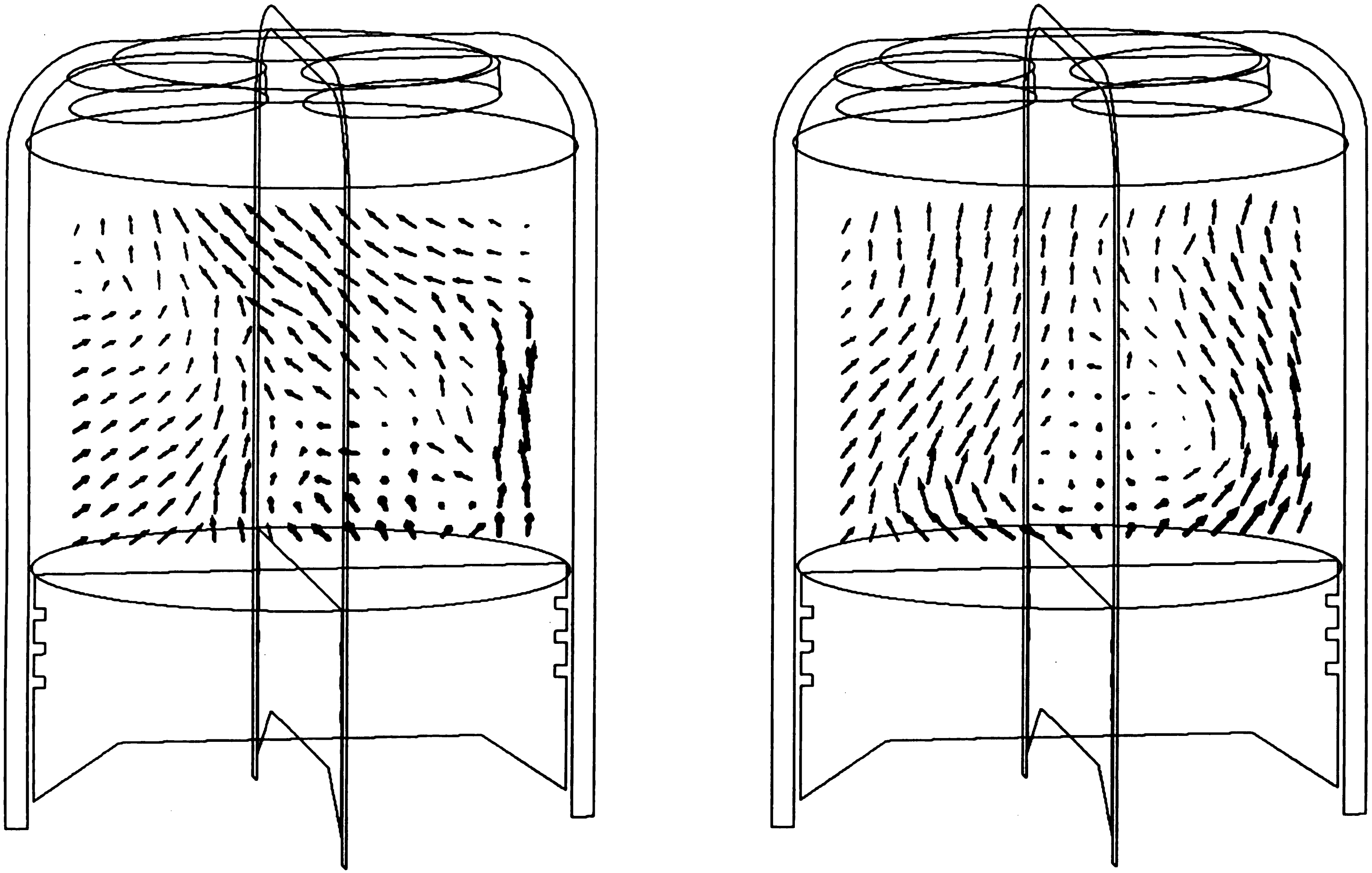

Figure A12: Vector fields for Plane 2, Configurations M and N, at 210.8 degrees.

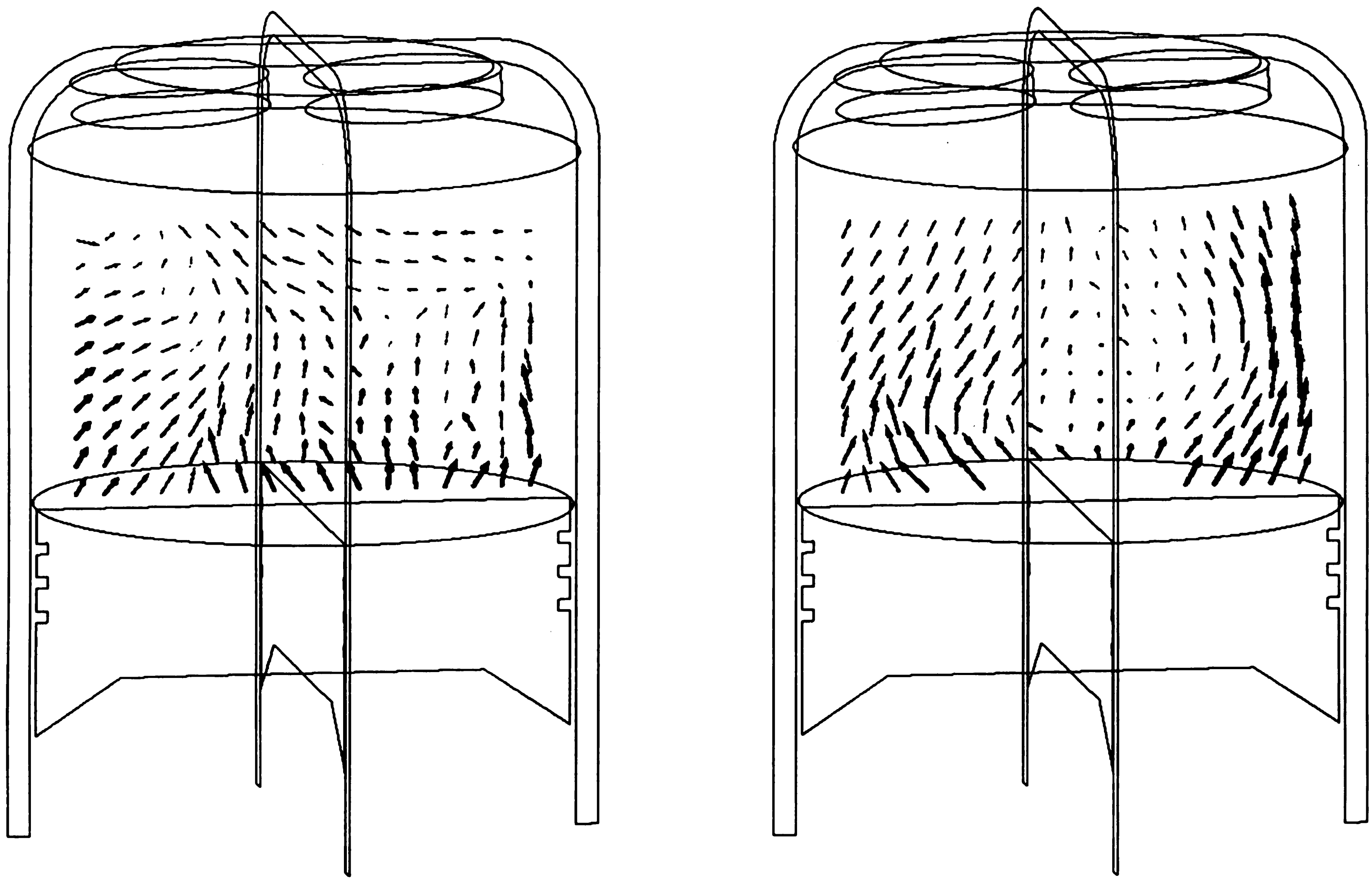

**Figure A13: Vector fields for Plane 2, Configurations M and N, at 240.3 degrees.**

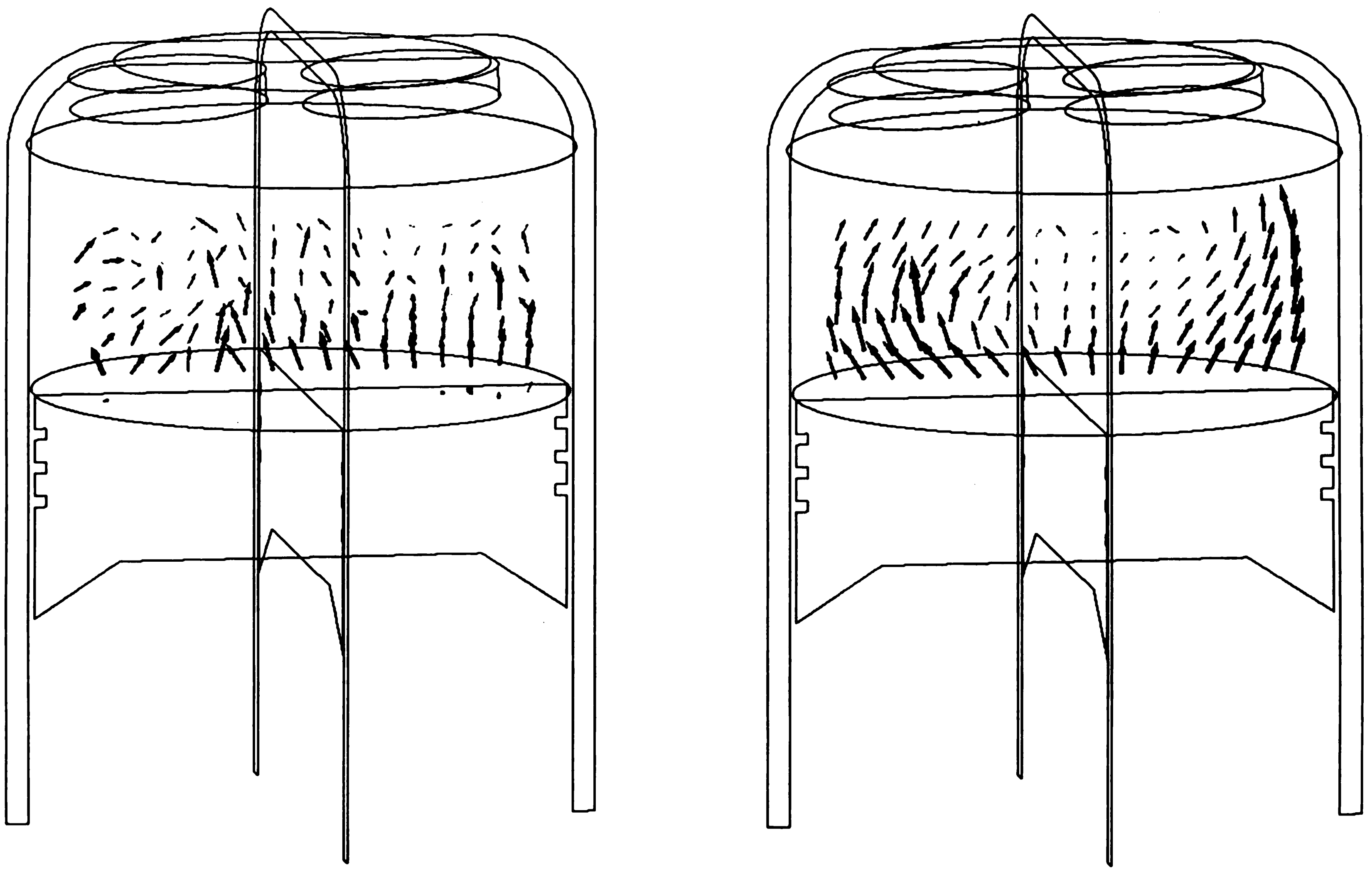

**Figure A14: Vector fields for Plane 2, Configurations M and N, at 269.8 degrees.**

# APPENDIX B

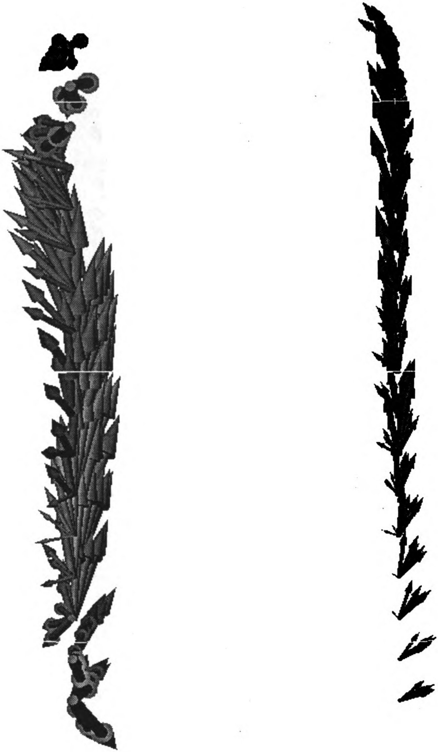

**Figure B1. Configuration M, Plane 1 from the +Y direction.**
**a) 119 degrees** **b) 227 degrees.**

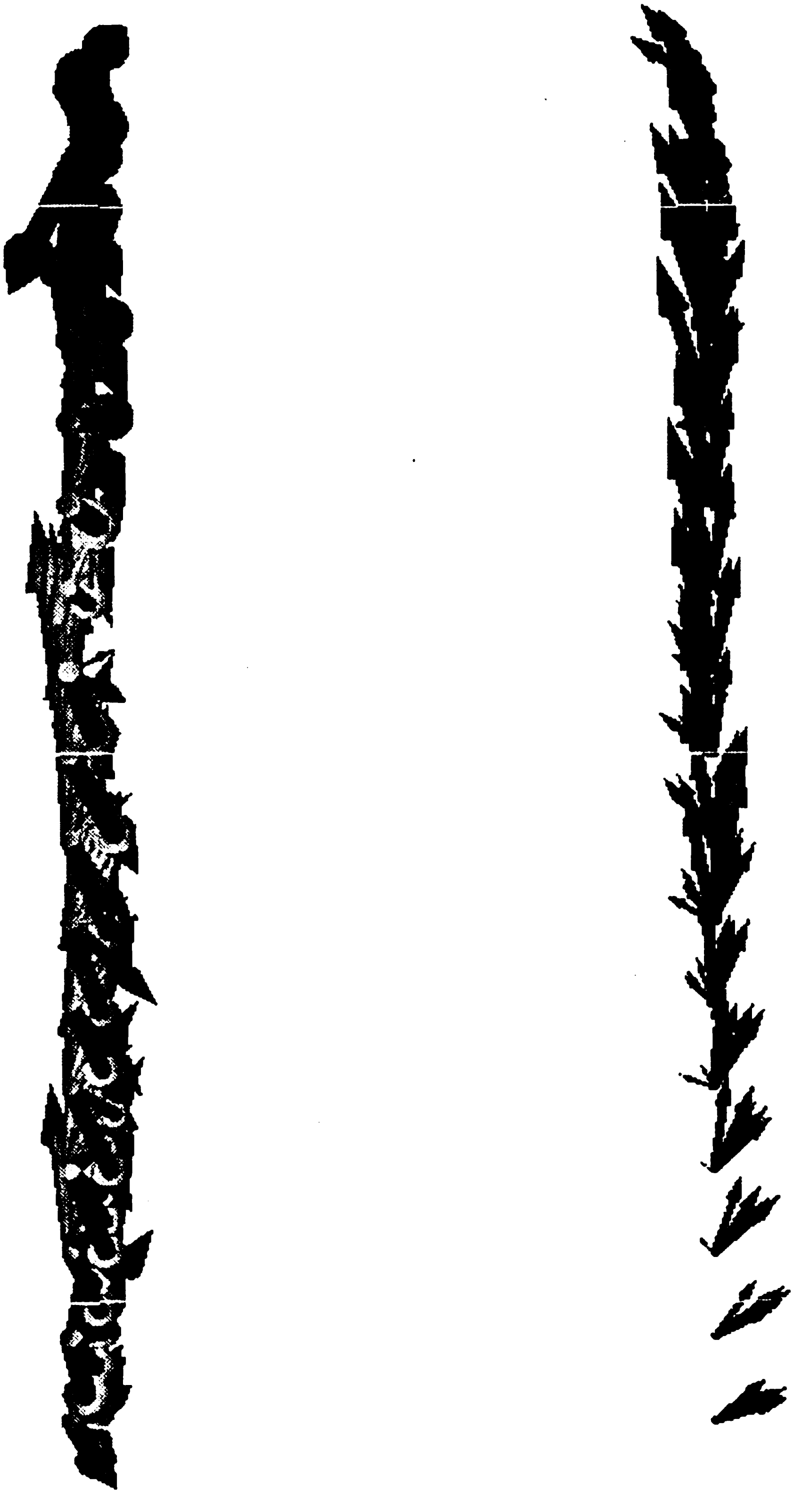

**Figure B2. Configuration N, Plane 1 from the +Y direction.**
**a) 119 degrees b) 228 degrees.**

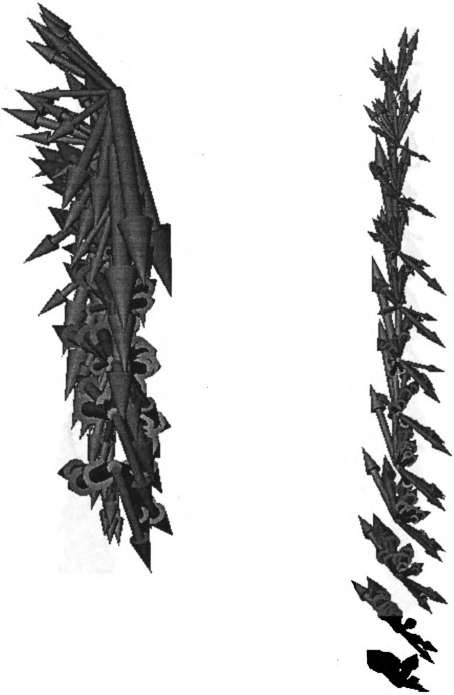

**Figure B3. Configuration M, Plane 1 from the +Z direction.**
**a) 108 degres** **b) 220 degrees**

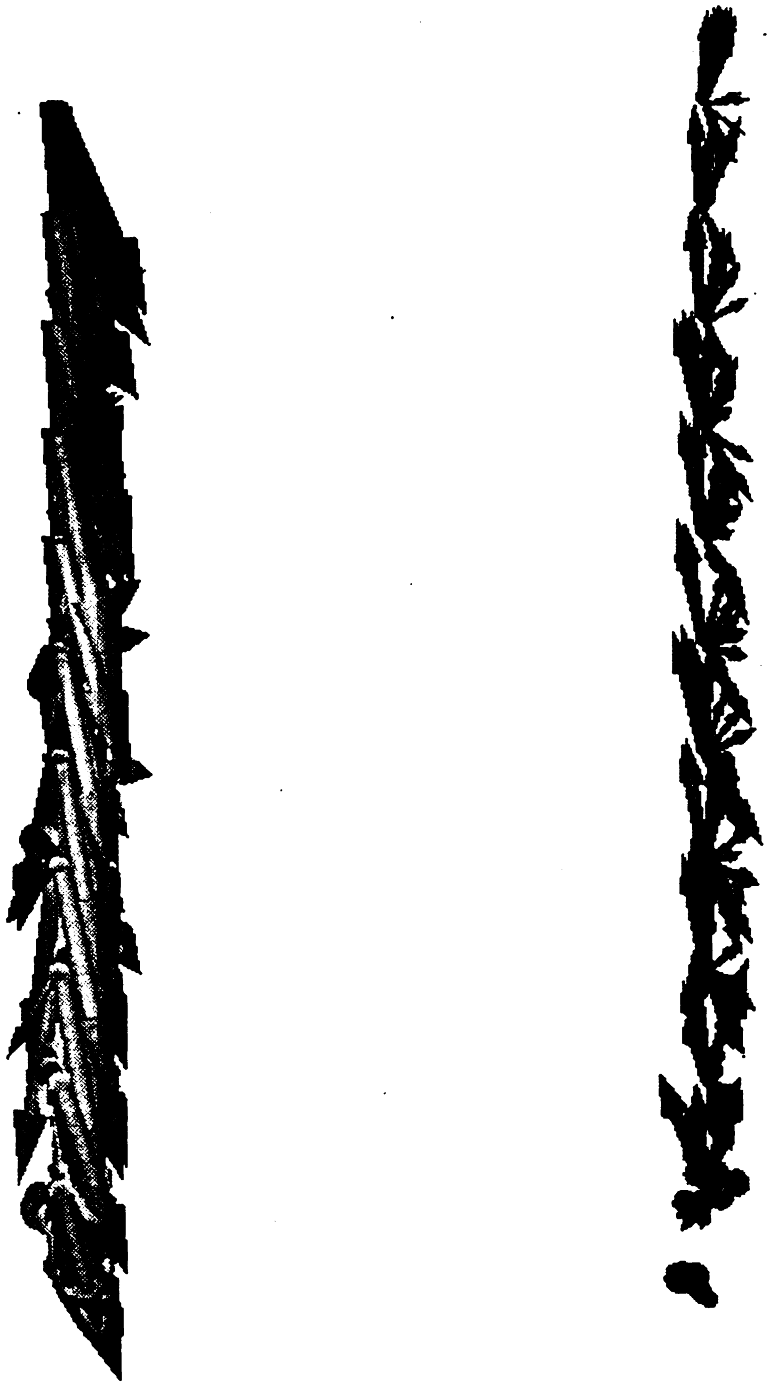

Figure B4. Configuration N, Plane 1 from the +Z direction.
a)135 degrees b)220 degrees.

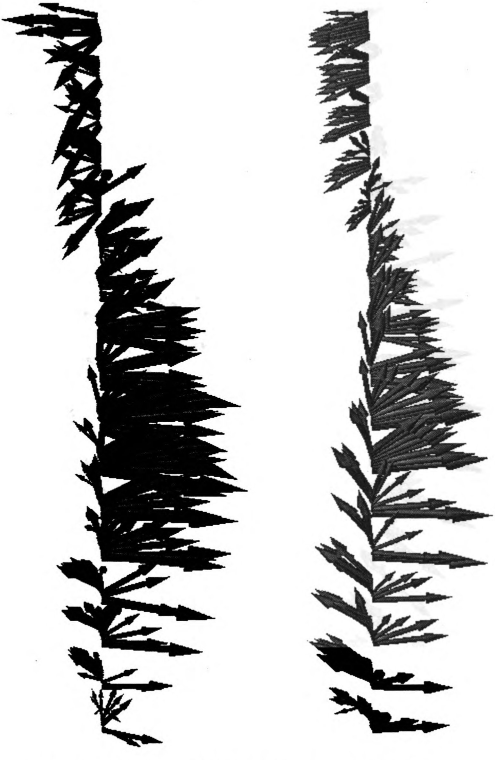

**Figure B5. Configuration M, Plane 2 from the +Y direction.**
**a) 139 degrees** **b)183 degrees.**

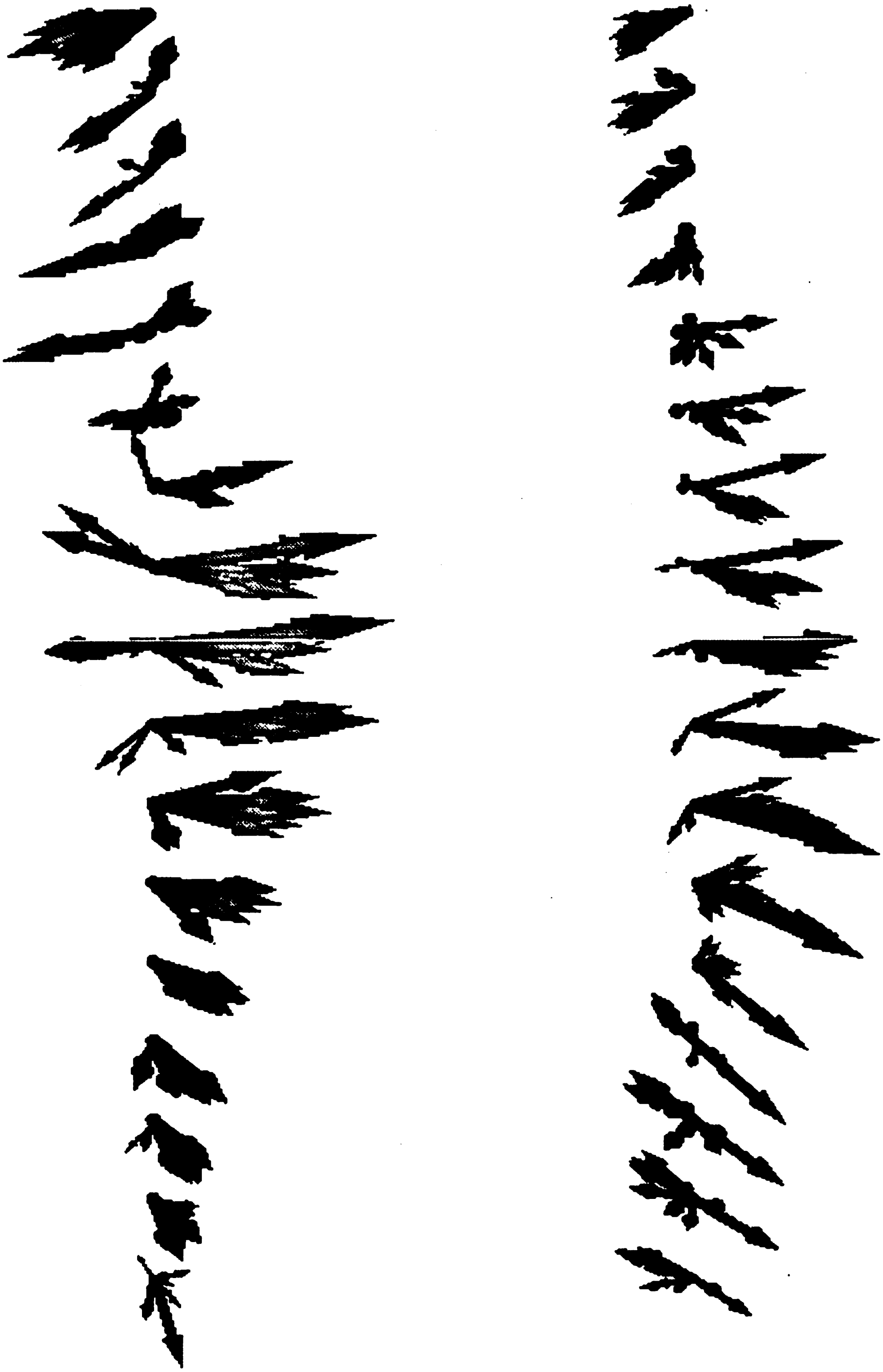

**Figure B6. Configuration N, Plane 2 from the +Y direction.**
**a) 139 degrees** **b) 183 degrees.**

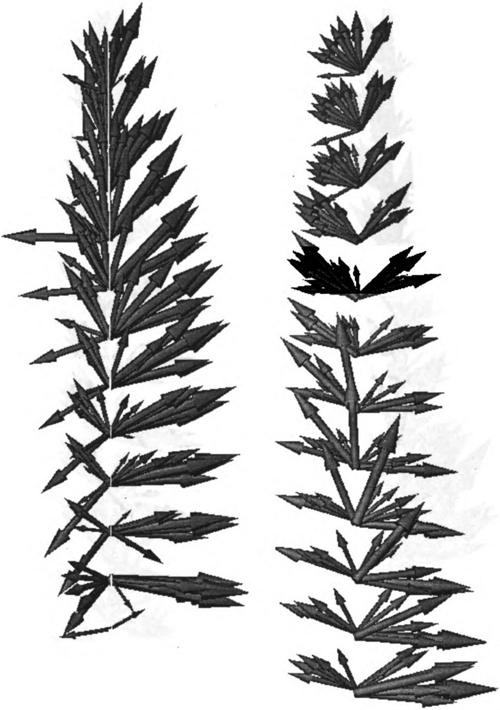

Figure B7. Configuration M, Plane 2 from the +X direction.
a) 135 degrees b) 204 degrees.

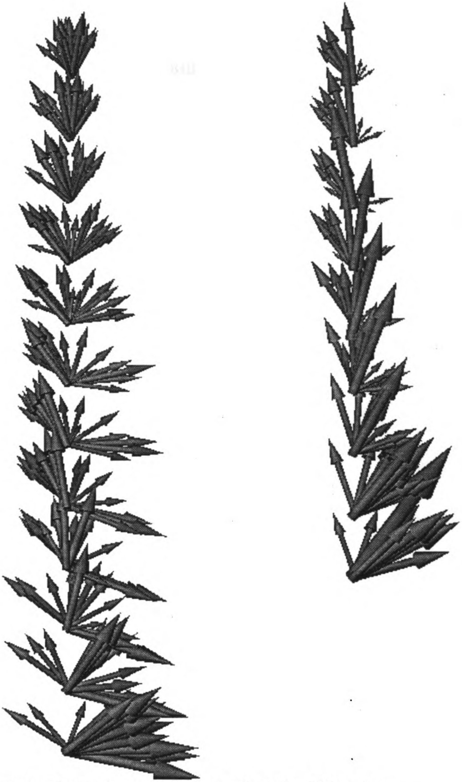

Figure B8. Configuration N, Plane 2 from the +X direction.
a) 203 degrees b)251 degrees.

# BIBLIOGRAPHY

## BIBLIOGRAPHY

1. Haworth, D.C., El Tahry, S.H., Huebler, M.S., Chang, S., "Multidimensional Port-and-Cylinder Flow Calculations for Two- and Four-Valve-Per-Cylinder Engines: Influences of Intake Configuration on Flow Structure." SAE Paper 900257, 1990.

2. Yoo, S.C., Lee, K., Stuecken, T., McCarrick, D., Schock, H., Hamady, F., LaPointe, L., Keller, P., Hartman, P., "An Experimental Study of In-Cylinder Air Flow in a 3.5L Four-Valve SI Engine by High Speed Flow Visualization and Two-Component LDV Measurement." SAE Paper 930478, 1993.

3. Yoo, S.C., Lee, K., Novak, M., Schock, H., Keller, P., "3-D LDV Measurement of In-Cylinder Air Flow in a 3.5L Four-Valve SI Engine." SAE Paper 950648, 1995

4. Schock, H., Hamady, F., LaPointe, L., DeFilippis, M., Stuecken, T., Gendrich, C., "High Frame Rate Flow Visualization and LDV Measurements in a Steady Flow Cylinder Head Assembly.", SAE Paper 910473, 1991

5. Mattavi, James N., "Effects of Combustion Chamber Design on Combustion in Spark Ignition Engines." SAE Paper 821578, 1982.

6. Sinnamon, J.F., Groff, E.G., "The Effects of Ignition Location in a Swirl Field on Homogeneous-Charge Combustion." SAE Paper 821221, 1982

7. Heywood, John B., "Fluid Motion Within the Cylinder of Internal Combustion Engines - The 1986 Freeman Scholar Lecture." Journal of Fluids Engineering, March 1987, Vol. 109.

8. Sierens, R., Snauwaert, P., "Experimental Study of the Swirl Motion in Direct Injection Diesel Engines Under Steady State Flow Conditions by LDA", SAE Paper 860026.

9. Henriot, S., LeCoz, J.F., Pichon, P., "Three-Dimensional Modeling of Flow and Turbulence in a Four-Valve S.I. Engine - Comparison with LDV Measurements." SAE Paper 890843, 1989

10. Endres, H., Neuber, H.J., Wurms, R., "Influence of Swirl and Tumble on Economy and Emissions of Multi-Valve SI Engines." SAE Paper 920516, 1992.

11. Coghe, A., Brunello, G., Gamma, F., Mauri, M., Culderini, F., Antoni, L., " In-Cylinder Air Flow Measurements by Laser Velocimetry under Steady-State Flow Conditions." SAE Paper 850123, 1985

12. Rask, R.B., "Laser Doppler Anemometer Measurements in as Internal Combustion Engine." SAE Paper 790094, 1979

13. Taylor, Charles F., The Internal Combustion Engine in Theory and Practice, Vol. 1 & 2, Second Edition, Revised. The MIT Press, Cambridge, MA, 1992.

14. Heywood, John B., Internal Combustion Engine Fundamentals. McGraw-Hill, New York, NY, 1988.

15. Foss, John F., and Potter, Merle C., Fluid Mechanics. Great Lakes Publishing, Okemos, MI, 1975.

16. White, Frank M., Viscous Fluid Flow, Second Edition. McGraw-Hill, New York, NY, 1991.